# ANTI-CANCER DRUG DELIVERY USING METAL ORGANIC FRAMEWORKS (MOFs) AND ULTRASOUND

by

Mihad Ibrahim

A Thesis Presented to the Faculty of the
American University of Sharjah
College of Engineering
in Partial Fulfillment
of the Requirements
for the Degree of

Master of Science in
Chemical Engineering

Sharjah, United Arab Emirates

May 2016

## Approval Signatures

We, the undersigned, approve the Master's Thesis of Mihad Ibrahim.

Thesis Title: Anti-cancer Drug Delivery Using Metal Organic Frameworks (MOFs) and Ultrasound.

| **Signature** | **Date of Signature** (dd/mm/yyyy) |
|---|---|
| _____ | _____ |
| Dr. Ghaleb A. Husseini<br>Professor, Department of Chemical Engineering<br>Thesis Advisor | |
| _____ | _____ |
| Dr. Rana Sabouni<br>Assistant Professor, Department of Chemical Engineering<br>Thesis Co-Advisor | |
| _____ | _____ |
| Dr. Dana Abouelnasr<br>Associate Professor, Department of Chemical Engineering<br>Thesis Committee Member | |
| _____ | _____ |
| Dr. Ana M. Martins<br>Senior Research Assistant, Department of Chemical Engineering<br>Thesis Committee Member | |
| _____ | _____ |
| Dr. Naif Darwish<br>Head, Department of Chemical Engineering | |
| _____ | _____ |
| Dr. Mohamed El-Tarhuni<br>Associate Dean, College of Engineering | |
| _____ | _____ |
| Dr. Leland Blank<br>Dean, College of Engineering | |
| _____ | _____ |
| Dr. Khaled Assaleh<br>Interim Vice Provost for Research and Graduate Studies | |

# Acknowledgements

First and foremost**,** I would like to thank the American University of Sharjah for granting me a graduate teaching assistantship. It was a wonderful opportunity to work as a teaching assistant while pursuing my Master's program in Chemical Engineering. Also, I owe sincere thanks to my advisor, Dr. Ghaleb Husseini, for the inspiring guidance throughout the research process. Without his help, I could not solve the challenges which I faced in my work. I really appreciate his precise technical and scientific editing while reviewing my thesis. In addition, his continuous support pushed me to work hard. It was a pleasure for me to work with Dr. Ghaleb who was very generous with his time, knowledge and expertise.

Special thanks and appreciation are extended to my co-advisor, Dr. Rana Sabouni, who continuously supervised my experimental work. Her office was always open whenever I had an inquiry. Without her valuable advices and suggestions I would not be able to finish my experiments. Additionally, I thank her for the useful comments while writing my thesis.

I would like to gratefully thank my thesis committee members, Dr. Dana Abouelnasr and Dr. Ana Martins, for reviewing the thesis and providing useful remarks. I would also like to thank Mr. Thomas Job, the laboratory instructor in the Chemistry and Environmental Sciences department, and Mr. Ziad Sara, the chemistry laboratory specialist, for their assistance throughout my research. Furthermore, I acknowledge the University of Sharjah for their help with characterization techniques. Last but not least, I would like to thank my colleagues in the Drug Delivery Research Group for the useful and often rigorous discussions during our weekly meetings.

## Dedication

*To my beloved parents, dear brothers (Hussam & Mussab), darling sisters (Maram & Monya), wonderful cousins (Rayan & Shaimaa) and sincere friends.*

## Abstract

Cancer is defined as the uncontrolled growth of abnormal cells. Although billions of dollars have been spent on cancer research to develop its treatments, cancer still remains a major illness for mankind, partly due to the drawbacks of these treatments. In an attempt to address the shortcomings of conventional chemotherapy (low targeting specificity, severe side effects and poor pharmacokinetics), anti-cancer drug delivery systems are being extensively researched using various nanocarriers including liposomes, micelles, polyelectrolyte capsules and others. Among the recent nanoparticles investigated as drug delivery vehicles are metal organic frameworks which are defined as porous hybrid polymers that consist of metal clusters and organic ligands. They have certain features that promote their use as drug carriers. First, they are nontoxic and have the ability to carry high loads of the drug. Also, their sizes are suitable to control *in vivo* and *in vitro* drug release. In this thesis, two new metal organic frameworks were prepared from iron nitrate and 2,6 naphthalenedicarboxylic acid. The first metal organic framework (Fe-NDC-M) was synthesized in a microwave oven, while the second (Fe-NDC-O) was prepared in an electrical conventional oven. Both were characterized using X-ray diffraction, scanning electron microscopy, energy-dispersive X-ray and Fourier transform infrared spectroscopy techniques. Then, they were used to load calcein disodium salt (a model drug mimicking the anti-neoplastic agent doxorubicin). Both particles showed high loading efficiencies (greater than 98%). The release kinetics of the model drug in neutral phosphate buffered saline were investigated with and without acoustic irradiation. Without ultrasound, the release percentages from the loaded Fe-NDC-M and Fe-NDC-O at 37°C were found to be 2.3 and 4.9 %, respectively, after 10 min. These percentages increased significantly after applying 40-kHz ultrasound to reach 22.7 and 79.7 % for Fe-NDC-M and Fe-NDC-O, respectively. To confirm the ultrasound effect in triggering the release, the loaded Fe-NDC-M particles were exposed to another ultrasound frequency (20-kHz) at room temperature. After 10 min, the particles released 37.5% of the encapsulated model drug, compared to 1.7% without ultrasound.



**Search Terms:** ***cancer, chemotherapeutic agent, metal organic framework (MOF), loading, release, cytotoxicity.***

# Table of Contents

# List of Figures

# List of Tables

## List of Abbreviations

| | |
|---|---|
| **2,6 NDC** | 2,6 naphthalenedicarboxylic acid |
| **5-FU** | 5-fluorouracil |
| **BDC** | terephthalic acid |
| **CCM** | curcumin |
| **CPT** | camptothecin |
| **CTAB** | cetyltrimethylammonium bromide |
| **DDS** | drug delivery system |
| **DEF** | diethylformamide |
| **DMF** | dimethylformamide |
| **DOX** | doxorubicin |
| **$EC_{50}$** | the half maximal effective concentration |
| **EDS** | energy-dispersive X-ray |
| **EPR** | enhanced permeability and retention |
| **ESCP** | ethoxysuccinato-cisplatin |
| **FBS** | fetal bovine serum |
| **FTIR** | Fourier transform infrared spectroscopy |
| **$H_3$BTB** | 4,4',4'' benzenetribenzoic acid |
| **HIFU** | high intensity focused ultrasound |
| **HPLC** | high performance liquid chromatography |
| **$IC_{50}$** | the half maximal inhibitory concentration |
| **MIL** | Materials of Institut Lavoisier |
| **MOFs** | metal organic frameworks |
| **MTBS** | methyltributylammonium methyl sulfate |
| **$NH_2$-BDC** | 2-aminoterephthalic acid |
| **NIM** | nimesulide |
| **NMR** | nuclear magnetic resonance |
| **PBS** | phosphate buffered saline |
| **SBF** | stimulated body fluid |
| **SEM** | scanning electron microscopy |
| **TEM** | transmission electron microscopy |
| **TGA** | thermogravimetric analysis |

| | |
|---|---|
| **TPT** | topotecan |
| **US** | ultrasound |
| **XRD** | X-ray diffraction |
| **ZIFs** | zeolitic imidazole frameworks |

# Chapter 1. Introduction

This chapter discusses general information about cancer, and its treatments. It also explains the mechanisms of targeting anti-cancer drugs using nanocarriers and the use of ultrasound in drug delivery. The last section lists the objectives of this thesis.

## 1.1. Background

Cancer is a deadly disease characterized by the rapid growth of abnormal cells in the body [1]. Its recent spread is attributed in part due to the rapid growth of population and the bad lifestyle habits including smoking, eating fast food and the lack of physical exercise [2]. In 2007, cancer killed about 7.9 million people all over the world and this number is increasing [3]. About 14.1 million new cancer cases were diagnosed in 2012 and 8.2 million deaths were reported by the International Agency for Research on Cancer [4]. Further epidemiological studies were carried out and showed that the number of cancer mortalities could reach 13.1 million by 2030 [5]. There are several types of carcinomas including breast, colon, liver, lung [5], colorectal, gastric, ovarian, soft tissue sarcoma and others [6]. The most common cancer spreads among males is lung cancer, while breast cancer is the predominant cancer among females [4].

There are essential differences between cancer and normal cells. Cancer cells grow quickly and their number can exceed the number of normal cells in the organ, forming a tumor. More dangerously, some of diseased cells can break away from the tumor and move through the blood stream to other parts of the body. So, they may migrate among the normal cells and start proliferating in a new location. Contrary to malignant tissue, when normal cells divide, an equal number dies in the process [7]. The tumorigeneses of certain cancers are shown in Figure 1 [8].

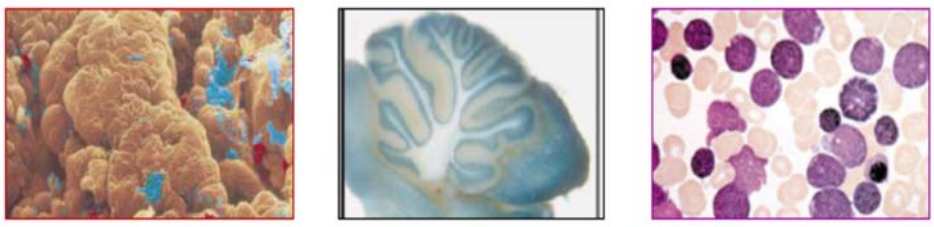

Figure 1: Tumorigenesis of colon carcinoma (left), medulloblastoma (middle) and leukemia (right) [8].

Despite differences in proliferation and multiplication, both cancer and normal cells are still human cells. Biochemical properties at the subcellular level related to the cell's surface are used to distinguish between them [7]. Cancer is seen as masses accumulating in tissues, but precisely, it is a cellular disease that starts with one cell mutating and then proliferating [9]. The first difference between cancer and normal cells is that normal cells form a monolayer (like a sheet) in the tissue, whereas cancer cells accumulate into multilayers [10]. Also, cancer cells have some outcrops on their surfaces which are not found in normal ones [7]. The last distinction is that various cancer cells have the ability to eliminate protease enzymes which are responsible for the protein digestion process [11]. The effect of these enzymes is to stimulate the cells to grow and in their absence, normal cells stay inactive [12].

The biochemical differences mentioned above could be useful in cancer treatment. They might open new methodologies to discover therapies that target cancer cells preferentially, while sparing the normal cells.

### 1.2. Cancer Treatment

There are different ways to control and treat cancer depending on its stage, location and the health of the patient [13]. Solid cancer tumors are resected surgically and afterwards, the patient is exposed to radiation therapies to get rid of any cancer cells not removed by surgery. The principal disadvantage of this method is that some of the tumors/tumor cells may not be removed completely and hence are capable of spreading beyond the diseased tissue or organ causing metastasis [14].

In 1900 and after clearly understanding the progress of the tumors, the German chemist, Paul Ehrlich, introduced the new term of "chemotherapy" and defined it simply as treating diseases with chemicals [15]. He carried out experiments on animals to examine the effect of various chemicals against cancer [15]. In his trials, the chemotherapy was considered a "dye therapy" [16] as he tried to use aniline dyes and alkylating agents, but unfortunately all of his attempts failed in regressing tumor growth. Until the 1960s, the prevalent treatment for cancer was surgery and radiotherapy [15].

After several studies, it was observed that many cancers could not be treated using these treatments (resection/radiotherapy) and they were ineffective in controlling the metastasis into other organs. On the other hand, it was shown that

adding a chemotherapy regimen to the traditional treatments could in some cases solve their drawbacks even if the cancer was in an advanced stage [15]. The main effect of the chemotherapy is to prevent the proliferation of cells, thus it affects both cancerous and healthy tissues [17]. This cancer treatment modality proved to be promising in patients suffering from breast cancer as the results revealed that the toxicity in the infected tissues was higher than in the normal ones [15].

The development of anti-cancer chemotherapy started in the 1930s after the First World War utilizing murine tumors experiments [6]. It was shown that when murine tumors were exposed to a dose of sulfur mustard gas followed by nitrogen mustard, a fast remarkable shrinking of the tumor occurred. After a decade, Goodman, Gilman, Allen and Philips investigated the effect of nitrogen mustard on tumors [18] and suggested the use of low doses of hydrochloride salt solution of nitrogen mustard injections to restrict and reduce the size of lymphatic tumors [6]. After 20 years of the investigation, the first *in vivo* experiments were carried out by Gilman. The results showed a noticeable effect of the cytotoxic drug (nitrogen mustard) on the lymphoid tissues [18].

These ideas assisted in investigating other drugs for their anti-cancer activity. The conclusion of these experiments was that the abnormal cells forming the tumor are more sensitive to the agent used. Further studies were done to test nitrogen mustard as a cytotoxic agent. The mechanism of drug delivery in this case was dictated by the effect of nitrogen mustard which covalently linked alkyl group with deoxyribonucleic acid (DNA) on purine [6]. The site at which cross-links formed matched where cancer cells died [19]. One of these alkylation agents is cyclophosphamide and is used to treat certain types of cancer including leukemia, lymphomas and some solid tumors. It was observed that cyclophosphamide had a short term treatment and cancer cells started resisting this chemotherapy treatment quickly [6].

In the late 1940s, a new anti-tumor drug, namely methotrexate, was discovered [6]. Injections of this chemotherapeutic agent limited the rapid growth of cancerous cells of acute lymphoblastic leukemia (especially in children) [6] in which proliferation is mainly stimulated by folic acid [20]. It is currently being used to treat osteosarcomas (malignant tumors in the bones) and lymphomas [21]. Although this therapy was effective in controlling the tumor, it had the same problem of

cyclophosphamide and cancer cells drug resistance was observed during the early stage of treatment [6]. Improving therapies to fight cancer did not stop and in 1962 another chemotherapeutic agent, 5-fluorouracil, was discovered [6]. It is currently being used in the treatment of colorectal, breast and gastric cancers [6, 22]. In the 1960s, a combination of cytotoxic therapies has been explored and specified for certain types of cancer including cisplatin which was researched as an anti-neoplastic agent in testicular cancer treatment [6].

Recently, many cytotoxic drugs appeared as a result of developing the chemotherapeutic agents discovered in the 1950s and 1960s [6]. Doxorubicin (DOX) is one of them and is capable of treating osteogenic sarcoma, chronic myelogenous leukemia, Hodgkin's lymphoma and soft tissue sarcoma [23]. Although many chemicals were developed and helped in treating cancer, they had severe side effects on the normal healthy cells. A new cancer therapy utilizing namely anti-hormonal drugs appeared in the 1960s [6]. Tamoxifen was the first to be used clinically in the 1980s in the treatment of breast cancer. Then, other drugs were developed for breast and prostate tumors [6].

Over the past two decades and after understanding the nature and the interaction between anti-cancer drugs and the tumors, nanotechnology applications have been utilized to target these drugs, and anti-cancer drug delivery systems have been developed using nanocarriers instead of simpler materials [24]. The purpose of their use is to avoid some of the drawbacks of chemotherapeutic agents including poor targeting specificity, burst effects due to high doses, insufficient information about the drug disposition in the body (poor pharmacokinetics) [25] and drug resistance after repeated exposures [26]. These nanomaterials should be non-toxic, stable *in vitro* and *in vivo* environments, biodegradable and have controllable drug distribution and release [27].

### 1.3. Mechanisms of Targeting Anti-cancer Drugs

There are two main mechanisms proposed to target anti-cancer drugs using nanocarriers: “passive” and “ligand” (also referred to as “active”) targeting [24]. The concept of the passive targeting is based on the leaky microvasculatures of cancer tumors, responsible for a unique phenomenon called enhanced permeability and retention (EPR) that is very advantageous when designing drug delivery systems [28].

The EPR effect was explained in 1986 by Maeda and coworkers when they discovered that large molecules (with molecular weight greater than 40-50 kDa), such as proteins and polymers, accumulate effectively and are retained in cancer tissues for a longer period of time than in normal tissues [29]. Tumors appear to grow fast as enough oxygen and nutrients are capable of penetrating easily in the defective and leaky blood vessels [30, 31].

The EPR effect has been widely utilized in drug delivery and to target chemotherapeutic agents encapsulated in nanocarriers including liposomes, polyelectrolyte capsules, micelles and others [32]. The most important factor affecting the efficiency of the passive targeting of anti-cancer drug carriers is their particle size which should be in the range of 20–200 nm to permeate easily through the gaps between the blood microvessels of cancer cells [28]. Other researchers have reported that the size of these fenestrations may reach 800 nm in size [33] or 2000 nm, depending on the localization, type and environment of the cancer cells [34]. Generally, most of the tumors have microvessels with pore cutoff size ranging between 380 and 780 nm [35]. The extent of tumor microvasculature heterogeneity, which differs with the type of cancer and from one tissue in the tumor to another, may affect the cellular uptake [36]. Liposomal doxorubicin (Doxil and Myocet), nanoparticle albumin-bound paclitaxel and other anti-neoplastic agents have already been used clinically to treat some cancers based on the passive targeting mechanism [28].

In ligand- or active-targeting, nanocarriers are functionalized by conjugating a ligand to their surface for which the cancer cells have particular receptors, which are not found or are found in much lower numbers in the normal cells [36]. Anti-cancer drug delivery carriers targeted “actively” and approved clinically include liposomal oxaliplatin conjugated using transferrin glycoproteins and immunoliposomal doxorubicin functionalized by human monoclonal antibodies (mAb), whereas several ligand-targeted therapeutics are currently in preclinical trials [28].

One of the recent nanoparticles investigated as effective drug carriers are metal organic frameworks (MOFs) [37]. They are defined as hybrid polymers that consist of metal salts (clusters) and organic compounds (linkers) [38]. Generally, MOFs have well-known crystalline structures with high surface areas that vary from 1,000 to 10,000 $m^2/g$ and high porosity (the volume of pores may exceed 50% of the

total volume) [39]. Some have additional features that promote their use in the biomedical field as drug carriers, including non-toxicity, biocompatibility, ability to entrap high loadings of the drug (because of their porous nature) and their sizes are suitable for *in vivo* drug release. They can be synthesized from some metals (such as iron, manganese, copper and zinc) which are found in blood plasma. It is worth mentioning here that nanoparticles based on iron oxide have been proven to be non-toxic [40].

### 1.4. Ultrasound in Anti-cancer Drug Delivery Systems

Recently, ultrasound (US) has been introduced as a modality to induce drug delivery from nanovehicles [41, 42]. The main advantage of applying US is to enhance the drug release from these nanocarriers and enhance its transport into the cytosol of tumor cells via sonoporation [43]. As a result of acoustic oscillation (ultrasound waves), drug transport increases. Sonoporation implies the increase in vessel permeability which in turns enhances the cellular uptake of drug nanocarriers [41, 44].

Two potential mechanisms/effects of acoustically activated drug delivery could be at play: i.e. thermal and nonthermal effects [41, 44]. Thermal effects deal with the interaction between US and biological tissues due to a localized temperature increase in the tissues which occurs as a result of absorbing acoustic energy by applying high intensity focused ultrasound (HIFU) [41, 45]. The temperature rise, which may reach 40 – 43°C, increases the membrane permeability by destabilizing the phospholipid bilayer. This phenomenon is called hyperthermia and it has been reported as the perpetrator behind cancer cells eradication and enhancing the cellular uptake of anti-neoplastic agents [46, 47]. To achieve hyperthermia using US, HIFU with frequencies ranging between 0.8 and 3.5 MHz is usually used [48].

The nonthermal mechanism of acoustic irradiation is due to mechanical and cavitation effects. The mechanical effect involves the motion of fluid and the nanocarrier via pressure waves or acoustic streaming, both of which have the capability of increasing the drug transport in the cells [41]. Alternatively, cavitation is defined as the formation and oscillation of very small gas bubbles (microbubbles) in tissues due to US-induced vibrations [49]. This generates high stress on the cell

membranes and the nanocarrier, resulting in the possible collapse and release of the drug [45].

Despite the extensive use of US in drug delivery when using several types of nanocarriers, including nanoemulsions, liposomes, micelles and polymeric nanoparticles, to the best of the author's knowledge it has not been previously applied to releasing encapsulated drug from MOFs [41, 45]. This thesis presents the first study of the effect of US on the drug release kinetics from MOFs.

## 1.5. Thesis Objectives

The main objectives of this thesis are:

I. To synthesize two new MOFs from iron nitrate and 2,6 naphthalenedicarboxylic using two synthesis routes: a) by mean of microwave irradiation (Fe-NDC-M) and b) solvothermally using a conventional electrical oven (Fe-NDC-O).

II. To characterize the resulting MOFs using X-ray diffraction (XRD), scanning electron microscopy (SEM), energy-dispersive X-ray (EDS) and Fourier transform infrared spectroscopy (FTIR) analytical techniques.

III. To load calcein disodium salt (model drug) in the prepared MOFs and determine the loading efficiencies.

IV. To investigate the release kinetics of the model drug from the loaded MOFs at 37°C without ultrasound and compare them with the 40-kHz ultrasound-triggered release**.**

V. To study the release behavior of the model drug from the loaded Fe-NDC-M at room temperature without ultrasound and after exposure to 20-kHz US.

The following chapter (Chapter 2) presents a literature review about MOFs with a focus on their use as anti-cancer drug carriers. In Chapter 3, the materials and methodologies used in the experimental work of this research are explained in details. Finally, the results of the characterization techniques as well as the loading and release experiments are discussed in Chapter 4.

# Chapter 2. Literature Review

The history of discovering MOFs, synthesis routes, first MOFs used as drug carries and a detailed review about MOFs as anti-cancer drug carriers are presented in this chapter.

## 2.1. History of Open-Framework Coordination

The first open-framework coordination was synthesized by Hofmann and Kspert in 1897 [50]. They prepared a hybrid network of $Ni(CN)_2(NH_3).C_6H_6$ crystals. After several decades, Pfeiffer and Feigl ended up with a 2-dimensional polymer consisting of one nickel molecule linked to two cyanide groups, ammonia and a benzene ring as depicted in Figure 2.

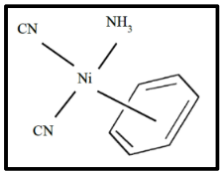


Figure 2: The structure of the crystal developed by Pfeiffer and Feigl [50].

In 1954, Powell and coworkers characterized $Ni(CN)_2(NH_3).C_6H_6$ using the X-ray diffraction (XRD) technique [50]. They found that the structure of the Hofmann model was not a 2-dimensional polymer. It is comprised of square flat Ni(II) metal centers surrounded by two cyano group $(CN)_2$ ligands, ammonia molecules and a benzene ring encapsulated inside these polymer sheets. Figure 3 represents a partial structure of these network crystals. Later, many researchers have modified the Hoffman complex and synthesized different networks using certain monomers with cyano group ligands and aromatic compounds. The structures of the resulting particles were determined by XRD and found to be crystals encapsulating the aromatic rings [50].

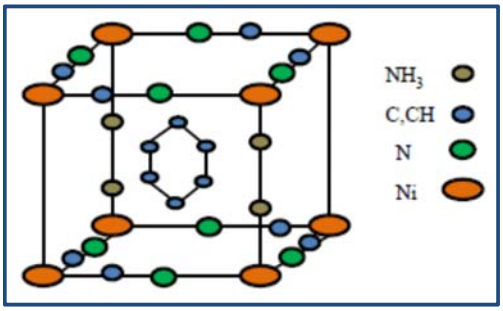


Figure 3: A partial structure of the crystal developed by Powell and coworkers [50].

## 2.2. Synthesis of Metal Organic Frameworks (MOFs)

MOFs are formed and tuned by combining any metal ions with organic ligands to get different structures and sizes. This chemical and physical variability renders MOFs useful in many applications including gas storage and separation, catalysis, purification of water, biomedical imaging, drug delivery and others [38, 51]. There are many routes to prepare MOFs with different structural designs. Most of them consist of metal clusters, bridging organic linkers and solvents, while others are solvent-free.

The metal salt and organic compounds can be mixed as solid powders in a solvent. Solutions of these solids can also be prepared first, and then mixed in the reactor [52]. The reaction occurs in the liquid phase after dissolving the reactants in the solvent which slows the reaction rate and absorbs the exothermic heat released [53]. Also, it helps in forming the crystals thus obtaining the required MOF structure. There are some factors affecting the selection of a suitable solvent including: reactivity, solubility, its phase at the reaction conditions, phase spilt, association or dissociation constants, selectivity as well as its heating and cooling properties [54]. The different synthesis routes are explained in the following sections.

**2.2.1. Low evaporation method.** MOFs are usually synthesized using two steps. The first step is the precipitation reaction of the dissolved solids at room temperature. Then, crystal growth starts with the slow evaporation of the solvent. Although this process does not require heat to evaporate the solvent, it is ineffective as it needs more time to complete compared to the other methods of synthesizing MOFs that will be discussed in the paragraphs below [52].

In 1989, Robson and coworkers designed the first organic network using an organic linker (instead of the CN group used in Hofmann complexes) [50]. They synthesized an infinite three-dimensional cationic MOF $\{Cu^{I}[C(C_6H_4.CN_4)]\}^{+}$. First, a tetrabromo derivative, 4,4',4'',4'''-tetrabromotetraphenylmethane ($C_{25}H_{16}Br_4$), was prepared from 2.55 g of iron, 12.3 g of tetraphenylmethane ($C_{25}H_{20}$) and 29 g of $Br_2$ dissolved in 100 mL of $CCl_4$. Then, the resulting tetrabromo derivative was recrystallized in dimethylformamide (DMF) (xylene can also be used) and reacted with 0.97 g of CuCN in 2.6 mL of DMF**.** After 4 h, 4,4',4'',4'''-

tetracyanotetraphenylmethane ($C_{29}H_{16}N_4$) was obtained by drying the mixture in vacuum at 100°C [55].

An amount of 22 mg of [$Cu(CH_3CN)_4BF_4$] and 40 mg of [$C_{29}H_{16}N_4.½\ C_6H_6$] were dissolved in a mixture of 1 mL of acetonitrile ($CH_3CN$) and 10 mL of nitrobenzene ($C_6H_5NO_2$). The solution was evaporated slowly and colorless crystals of {$Cu^I[C(C_6H_4.CN)_4]BF_4.(C_6H_5NO_2)$} were obtained. Some of the crystals were collected, washed with nitrobenzene and dried in air. The remaining particles were kept in the main solution to investigate their morphology using the X-ray crystallographic analysis and found to be porous diamond-like shapes encapsulating random $BF_4^-$ ions and nitrobenzene inside the cavities [55].

Figure 4 shows the structure of the MOF in which the larger circles represent the copper atoms, the rod-like units denote the organic linker ($C_{29}H_{16}N_4$) and the black lines denote the cavity with a volume of 700Å$^3$ ($BF_4^-$ ions and $C_6H_5NO_2$ are not shown in the structure). Utilizing this synthesis method, Robson and his group succeeded to design the first MOF and outlined a procedure to prepare porous solid polymers with well-defined sizes and shapes [55].

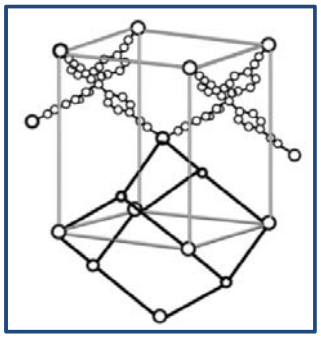

Figure 4: $\{Cu^I[C(C_6H_4.CN)_4]\}^+$ framework [55].

The second MOF was synthesized in 1994 using cadmium nitrate [$Cd(NO_3)_2$] and 4,4' bipyridine (4,4'-bpy) ($C_{10}H_8N_2$) that formed a two-dimensional square framework with porous structure as shown in Figure 5 [50]. To prepare this MOF, 2 mL of 4,4'-bpy (2.0 mmol) were dissolved in ethanol and 8 mL of aqueous cadmium nitrate (1.0 mmol) at room temperature and after 24 h, fine colorless crystals were collected [56]. The first trial to encapsulate a material in the pores of [$Cd(4,4'\text{-}bpy)_2(NO_3)_2$] was implemented to load o-dibromobenzene ($C_6H_4Br_2$). The encapsulation was confirmed by the single XRD technique and the structure of loaded MOF was found to be a two-dimensional graphite-like solid in two layers.

Each layer comprises a planar square of cadmium ion and 4,4'-bpy at the edges and $C_6H_4Br_2$ in the empty spaces. Figure 6 represents the structure of this complex [50].

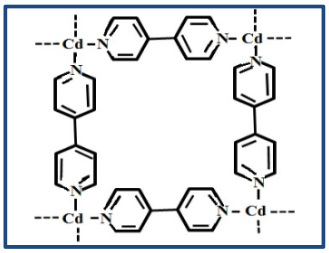

Figure 5: Structure of $[Cd(4,4'\text{-bpy})_2(NO_3)_2]$ [56].

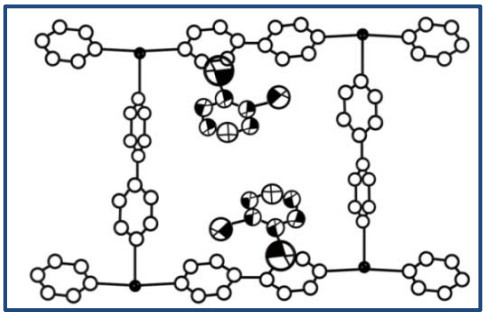

Figure 6: View of the complex $[Cd(bpy)_2](NO_3)_2(C_6H_4Br_2)_2$ [50].

**2.2.2. Solvothermal synthesis.** It is defined simply as any reaction occurring at elevated temperatures and pressures in a closed vessel, using organic or inorganic solvents [57]. Diethylformamide (DEF), DMF, ethanol, methanol and acetone are the most common solvents used [52]. There are important factors affecting the solvothermal synthesis and the resultant MOF structure including temperature, concentrations of the reactants (metal salt and ligand), the ligand length and bond angles, the geometries, the solubility of the solids in the solvent and the pH of the liquid mixture [58]. When the metal salt is dissolved in water, the process is called hydrothermal synthesis [52].

In 1995, Zaworotko and coworkers prepared another organic coordination molecule $\{[Zn(4,4'\text{-bpy})_2]SiF_6\}$ that has square cavities with a volume around 50% of the total volume [59]. First, 0.31 g of $[Zn(OH_2)_6]SiF$ was dispersed in 25 mL of benzene and 25 mL of in 1,4-dioxane ($C_4H_8O_2$). The mixture was heated using the Dean-Stark apparatus to remove the water and obtain $ZnSiF_6$ as a powder. About 25 mL of DMF were added and the whole mixture was heated in a rotary evaporator where most of the 1,4-dioxane and benzene evaporated. The remaining mixture was

cooled down and 0.31 g of 4.4'-bipyridine dissolved in 10 mL of 1,4-dioxane was added and heated for 30 min. Then, a yellow solution was observed and cooled at room temperature for 12 h, resulting in 0.48 g of colorless crystals of {[Zn(4,4'-bpy)$_2$]$SiF_6$}. The pores have a hydrophobic nature and thus can encapsulate hydrophobic materials only [59].

In the same year, Yaghi and his group have established the hydrothermal synthesis and applied it to synthesize a new metal network {[Cu(4,4'-bpy)$_{1.5}$]$NO_3$.($H_2O$)$_{1.25}$} [50]. They dissolved 0.17 g of Cu($NO_3$)$_2$.2.5$H_2O$, 0.04 g of 1,3,5-triazine (HCN)$_3$ and 0.17 g of 4,4'-bpy in 15 mL of deionized water. They have poured the solution in a closed stainless steel bomb and heated it in a furnace by increasing the temperature 5 degrees/min until it reached 140°C and then remained constant for 24 [60]. Then, the resulting mixture was cooled gradually at a rate of 0.1 degree/min and when the temperature has reached 90°C, it was kept constant for 12 h followed by cooling at the same rate to 70°C and held at this temperature for 12 h. Finally, it was cooled at a rate of 0.1 degree/min to the room temperature.

The single-crystal XRD analysis using the Siemens SHELXTL-PC software package showed the shape of the crystals as three-dimensional porous networks consisting of copper atoms at the corners which are connected by rod-like bipyridine rings**.** The voids between the networks are filled with the water and nitrate ions [60].

**2.2.3. Microwave-assisted irradiation method.** This method succeeded in reducing the time required for crystallization at different ranges of temperature without any deformations in the MOF structure. However, it was not used frequently because not enough information was available about the crystals morphology to evaluate the structural data obtained for the nanoparticles [58].

In 2006, Ni and Masel used this procedure to prepare three groups of MOFs, named IRMOF1 (zinc oxide with 1,4-benzenedicarboxylate), IRMOF2 (zinc oxide with 2-bromoterephthalic acid), and IRMOF3 (zinc oxide with 2-aminoterephthalic acid) [61]. The metal precursor and organic compound were dissolved in DEF and mixed for 15 minutes to get a homogenous solution. To synthesize IRMOF-1, 0.67 mmol of the metal precursor and 0.50 mmol of the organic linker were dissolved in 10 ml of DEF. One mL of the solution was poured into a closed Pyrex flask of 4 mL

volume and placed in a laboratory microwave synthesizer. After 25 seconds, the product was centrifuged and IRMOF-1 microporous particles were collected. The crystals were characterized by scanning electron microscopy (SEM) and their shapes were found to be small cubes that had sizes ranging between 3-5 micrometers as shown Figure 7 [61].

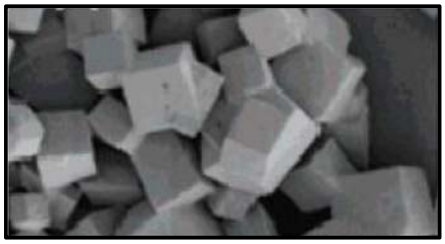

Figure 7: Crystals of IRMOF1 by SEM [61].

IRMOF-2 and IRMOF-3 were synthesized using the same steps with different amounts of metal salt, ligand and solvent [61]. The microwave strategy is somewhat similar to the solvothermal reaction and the particles produced have the same quality, but the microwave requires less time [52].

**2.2.4. Electrochemical synthesis.** This method of synthesis was investigated in 2005 by researchers in the Badische Anilin- & Soda-Fabrik (BASF) company in Germany [62]. They tried to use metal ions instead of metal salts to reduce the cost especially for large scale MOF production, because these ions are produced in the reaction medium that contains the dissolved organic linker and electrolytes. As a result of oxidation and reduction, hydrogen gas was formed and the metal ions were deposited on the cathode [62].

Protic solvents including methanol, ethanol, and isopropanol can be used to remove the deposited metal [62]. An example of MOF prepared using the electrochemical methods is $Cu_3(BTC)_2$ prepared from zinc oxide and 1,3,5-benzenetricarboxylic acid (BTC). When the metal was immersed in the electrolyte solution containing the organic ligand and a salt of methyltributylammonium methyl sulfate (MTBS), the electric voltage was produced and crystals of $Cu_3(BTC)_2$ grew due to the electrochemical reaction. The SEM technique was used to determine the size of the particles which were found to be in the range of 2 to 50 μm as shown in Figure 8 [63].

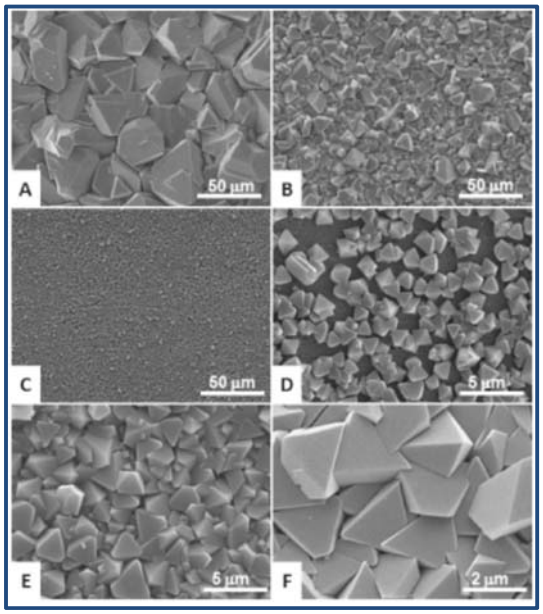


Figure 8: Crystals of $Cu_3(BTC)_2$ by SEM [63].

**2.2.5. Mechanochemical synthesis.** Recent studies reported this route as a solvent-free process that depends on a mechanical force to induce the chemical reaction that produces MOFs rapidly. Grinding the solid substances produces mechanical energy that breaks the bonds of the solids allowing the chemical reaction to take place, thus forming other intermolecular bonds of the produced crystals. Although this process is carried out without a solvent, a small amount of solvent is used with the solid mixture to aid in the grinding step, and thus the reaction proceeds at a faster rate [52].

Klimakow *et al.* synthesized two MOFs using copper acetate monohydrate cluster with BTC and the same cluster with 4,4',4'' benzenetribenzoic acid ($H_3BTB$) in ethanol [64]. The mixtures were prepared in a molar ratio of 3:2 and ground for 25 minutes in a conventional ball mill. The resulting MOF structures are shown in Figures 9 and 10 [64].

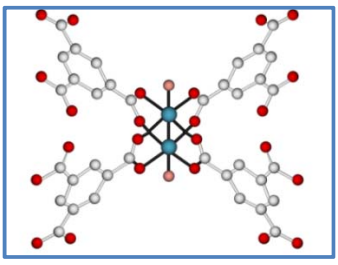

Figure 9: $H_3BTC$ metal organic framework [64].

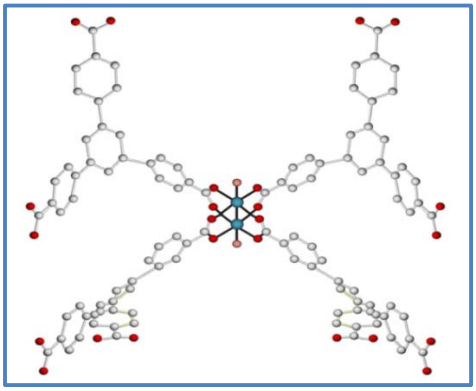

Figure 10: $H_3BTB$ metal organic framework [64].

**2.2.6. Sonochemical synthesis.** The routes of preparing MOFs have been developed to reduce the time of crystallization and get homogenous particle structures. Sonochemical synthesis is a rapid method in which high-energy ultrasound radiation is used as a driving force for the chemical reaction to produce micro- or nano-MOFs. The ultrasonic waves are cyclic mechanical vibrations that have frequencies between 20 kHz and 10 MHz [52]. When applied, they stimulate the reactant molecules to move rapidly and strike each other. As a result of the cyclic vibrations, bubbles start to grow in the liquid mixture of the metal salt, ligand and solvent. The size of these bubbles increases until they collapse and release their energy producing high temperatures and pressures in the process [52]. Due to the differences in the pressure and temperature of the new bubbles formed and the reaction mixture, MOF crystals grow quickly [65].

The first MOF prepared by the sonochemical procedure was synthesized from BTC and an aqueous solution of zinc acetate salt. The reactants were added into a mixture of water and ethanol and sonicated for a short time (less than 30 min). The produced particles [$Zn_3(BTC)_2$] had spherical structures with sizes ranging between 100-200 nm. It was observed that when the reaction time was increased to 30 and 90 min, the resulting MOFs looked like long needles with larger diameters (up to 900 nm) [62]. Sonochemical synthesis was applied to construct many other MOF networks such as MOF-5 ($Zn_4O$ nodes with 1,4-benzodicarboxylic acid), Fe-MIL-53 [$FeCl_3.6H_2O$ with terephthalic acid (BDC)] and HKUST-1 (copper nodes with BTC). This synthetic approach is environmentally friendly and effective in terms of the cost and energy (the reaction occurs at room temperature using ultrasonic irradiation). In

addition, it can produce high yields of homogeneous nanocrystals in shorter time compared with the other synthesis routes [62].

Using different metal salts and organic ligands, unlimited structures can be formed and used for different applications.

## 2.3. The First MOFs as Potential Drug Carriers

The first family of MOFs that can be used in drug delivery systems was investigated in 2006 by Horcajada and co-workers [66]. It consists of two groups called MIL-100 and MIL-101 (MIL is abbreviation of Materials of Institut Lavoisier). These two examples were synthesized using carboxylic acid groups as organic ligands and trivalent metals as clusters. The MIL family has many structural characteristics that promote its use as drug carriers including large pores with identified surface areas and its ability to form a hybrid network [66].

Horcajada and co-workers carried out experiments to study the kinetics of the ibuprofen (anti-inflammatory drug) loading and release using MIL-100 and MIL-101 complexes with chromium (Cr) [66]. MIL-100 was synthesized by mixing metallic chromium, BTC, hydrofluoric acid (HF) and water with a molar ratio of 1: 0.67: 1: 265. Then, the mixture was placed in a Teflon-lined bomb and heated gradually for 4 days at 220°C. The other MOF, MIL-101, was synthesized by heating a mixture of chromium (III) nitrate [$Cr(NO_3)_3 \cdot 9H_2O$], HF, BDC and water in a molar ratio 1: 1: 1.5: 280 for 10 h at 220°C in a Teflon-lined bomb calorimeter. To collect the particles, the mixture was cooled down, filtered and dried at 100°C in an oven for 24 h. Figure 11 shows the structure of Cr-MIL-100 and Cr-MIL-101 [66].

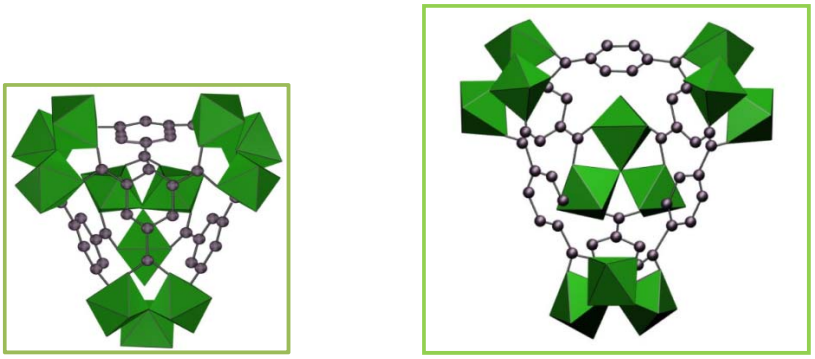

Figure 11: Cr-MIL-100 (left) and Cr-MIL-101 (right) [66].

To carry out the drug loading experiments, 100 mg of the dried particles were stirred in the presence of 10 mL of hexane containing 200 mg of ibuprofen for 24 h. The loading capacities were determined, using the elemental analyzer and X-ray fluorescence spectroscopy, to be approximately 0.35 g of ibuprofen/g of MIL-100 and 1.4 g ibuprofen/g MIL-101. Although the loadings of the carriers were relatively high, they did not affect the structure of the MOF when characterized by X-ray powder diffraction. The release was then observed and controlled under certain conditions and occurred completely within three and six days for MIL-100 and MIL-101, respectively, which was slow enough to reduce the side effects usually experienced by a patient taking the medication [66].

To investigate the release kinetics, 200 mg of the encapsulated drug were compressed by applying isostatic pressure of 3 MPa and uniaxial pressure of 2.75 MPa. Discs with a diameter of 13 mm were obtained and impregnated in a stimulated body fluid (SBF) at 37°C. High performance liquid chromatography (HPLC) was used to determine the concentration of the drug released in the SBF. It was found that the entire release from MIL-100 took 3 days, whereas it took 6 days in the case of MIL-101. Despite the efficiency of this administration route, the particles were synthesized using chromium which is toxic. Therefore, its application in drug delivery is restricted. Toxic chromium can be replaced by other metal ions including iron, copper, manganese, zinc and nickel which are nontoxic and are naturally found in the body [66].

Generally, the MIL constructs are hydrophobic polymers that are suitable for encapsulating hydrophobic drugs [67]. On the other hand, there are other MOFs with hydrophilic pores used to deliver cationic drugs. Recently, Rosi and coworkers have prepared a new MOF (bio-MOF-1) based on one of the purine derivatives called adenine ($C_5H_5N_5$) and zinc (II) ions and used it to encapsulate procainamide (antiarrhythmic drug) [68]. The MOF was prepared by dissolving 0.125 mmol of adenine, 0.375 mmol of zinc acetate dihydrate [$Zn(CH_3COO)_2 \cdot 2H_2O$] and 1 mmol of nitric acid in 1 mL of water and 13.5 mL of DMF. The mixture was placed in a capped vial and heated at 130°C for 24 h. Then, the resulting crystals were collected, washed 3 times with 3 mL DMF and dried for 30 min under argon [68].

To determine the drug loading, the MOF was soaked twice in an aqueous solution of 0.1 M of procainamide hydrochloride for 10 min and the solution was

removed. Then, the impregnation was performed for 24 h followed by solution removal. This step was repeated every 24 h for 15 days. The final loading was calculated from the thermogravimetric analysis (TGA) results and found to be 0.22 g of procainamide/g of loaded MOF. Furthermore, the release was investigated by adding 15 mg of the loaded drug to 1 mL of 0.1 M phosphate buffered saline (PBS) at pH 7.4 [68]. PBS is used in biological research, because its ion concentrations match those of the human body [69]. The complete release was observed by HPLC and occurred after three days. When the complexes were loaded in nanopure water (not PBS), the release achieved was only 20% of the amount inside the framework. It was an indicator that the main reason for the release was the cations in the saline solution, not the MOF [68].

As there are unlimited numbers of MOFs that can be synthesized, they should be selected carefully when used for medical applications. The toxicity and stability levels should be examined and determined before their usage.

### 2.4. MOFs as Anti-cancer Drug Carriers

Recently, metal organic frameworks as anti-cancer drug carriers have attracted attention, as they have shown less toxicity with high efficiency in terms of targeting chemotherapeutic agents [70]. In 2009, Lin and coworkers reported the loading of cisplatin prodrug in the nanoporous MOF, MIL-101 (Fe) [71]. Cisplatin and its derivatives are targeted anti-cancer therapies based on platinum metal and used effectively to cure testicular and ovarian cancer, but their level of toxicity can cause severe side-effects including nausea, nephrotoxicity and bone marrow suppression [72]. To reduce the unwanted side effects by controlling the release, one of the cisplatin derivatives called ethoxysuccinato-cisplatin (ESCP) prodrug, which treats many types of carcinomas including cancers of soft tissue, bones, muscles, sarcoma cancers and blood vessels [73], was loaded in a functionalized Fe-MIL-101 [71].

To synthesize the functionalized Fe-MIL-101, typical amounts of 1.38381 mmol of $FeCl_3 \cdot H_2O$ and 1.38381 mmol containing 17.5 mole% 2-aminoterephthalic acid ($NH_2$-BDC) [$H_2NC_6H_3$-1,4-$(CO_2H)_2$] and the remaining BDC were dissolved in 30 mL of DMF and heated to 150 °C for 15 min in a sealed microwave vessel using a HP500 microwave. Then, the resulting mixture, which contained the particles, was cooled down at ambient temperature and centrifuged. The particles were collected and

washed with ethanol and DMF to remove the excess reactants. It was found that 17.4 mol % $NH_2$-BDC incorporated with the metal to form the MOF [71].

The loading of the drug was carried out in two steps. First, 22 mg of ESCP and 9.3 mg of 1,1-carbonyldiimidazole [$(C_3H_3N_2)_2CO$] were dissolved in 3 mL of DMF and heated, under argon, at 60 °C for 1 hour followed by cooling to room temperature. The purpose of adding 1,1-carbonyldiimidazole is to activate the cisplatin. Then, 85 mg of the MIL-101 (Fe) was stirred with the solution at room temperature for 48 h and the loaded particles were collected by centrifugation and washed with ethanol and DMF. The washed particles were isolated from the solution by a dialysis technique against distilled water for 5 hours (the water was changed every 1 h). Figure 12 represents the SEM images of MIL-101 (Fe) before (left) and after the loading (right) [71].

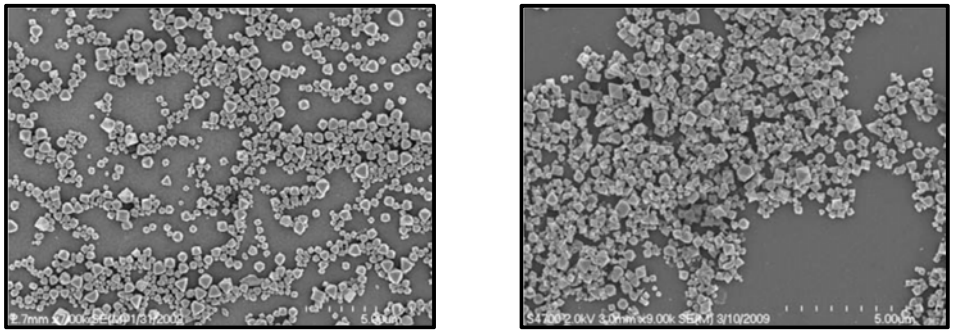

Figure 12: SEM images of MIL-101 (left) and after ESCP loading (right) [71].

The collected particles had the same structure of MIL-101 with the same diameter (200 nm) and 12.8 wt.% payload (mg encapsulated drug/mg MIL-101). In addition, the release was measured by a fluorescence spectrometer and completed after 1.2 h in PBS at 37°C. It was observed that the MOF particles were not stable and decomposed in the buffer solution; therefore the loaded nanocarriers were coated by a thin layer of sodium metasilicate ($Na_2SiO_3$) to slow the release [71].

The loaded Fe-MIL-101 nanoparticles were coated with sodium silicate as follows: 10 mg of the loaded nanoparticles were suspended in ethanol, centrifuged and then dispersed in 4 mL of water. Then, 47.5 mg of sodium silicate ($Na_2SiO_3.5H_2O$) were dissolved in 2 mL of water and HCl was added to get a neutral solution. This solution was added to the nanoparticles suspension and the entire mixture was diluted to 20 mL by adding water. The resulting suspension was stirred at 60°C for 3 h followed by centrifugation. The coated particles were washed with

ethanol and water, and dispersed in ethanol for further experiments. The release through the silica shell took 14 hours instead of 1.2 hour under the same conditions [71].

When the coated nanoparticles were used to treat HT-29 human colon adenocarcinoma cells, it showed slightly less cytotoxicity (the half maximal inhibitory concentration ($IC_{50}$) = 29 μM) compared to cisplatin ($IC_{50}$ = 20 μM). The loaded drug was activated and modified to target specific tumor cells in two steps. First, glutathione antioxidant ($C_{10}H_{17}N_3O_6S$) was used to activate the content of the silica shell inside the cells. Then, it was functionalized by attaching a cyclic peptide ($C_{27}H_{41}N_9O_7$) called c(RGDfK). The latter having an affinity towards $\alpha_v\beta_3$ integrin receptors found in many cancer cells [71].

To attach the peptide, the coated nanoparticles (cisplatin loaded in Fe-MIL101) were dispersed in ethanol with a concentration of 2 mg/mL and the c(RGDfK) solution was added to the suspension. The mixture was diluted by adding aqueous HCl to obtain a pH of 3 and then stirred for 1 day in the dark to conjugate the c(RGDfK). Figure 13 represents the attachment of (ESCP) through amino groups on $NH_2$-BDC particles [37].

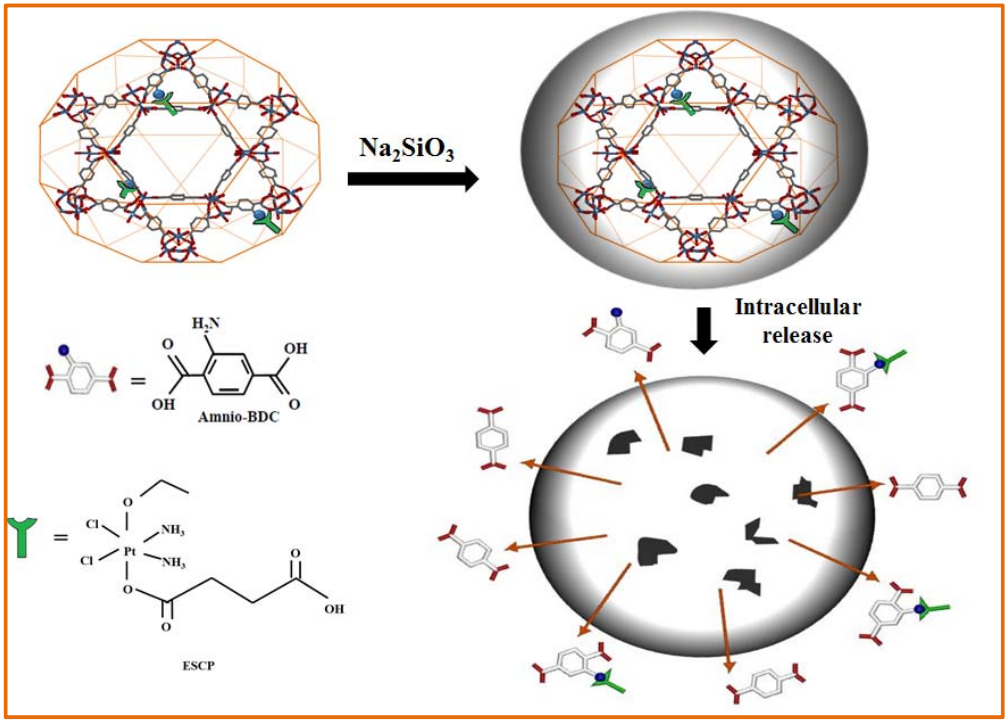


Figure 13: Attachment of (ESCP) through amino groups on $NH_2$-BDC particles [37].

The targeted particles were centrifuged, washed with and dispersed in ethanol. HT-29 human colon adenocarcinoma cells were targeted efficiently by the new modified therapy with cytotoxicity ($IC_{50}$=21 μM) similar to that observed with free cisplatin. The SEM image of the loaded drug after the coating and c(RGDfK) attachment is shown in Figure 14 [71].

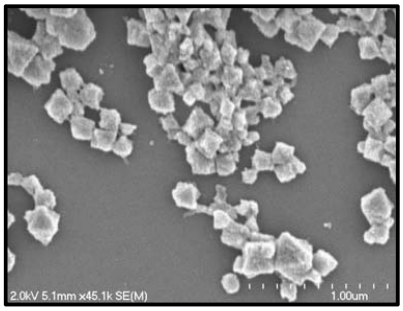


Figure 14: SEM image of the loaded drug after the coating and c(RGDfK) attachment [71].

Another chemotherapeutic agent reported to be loaded in nanoMOF is topotecan (TPT) which is a member of the cytotoxic drug family of camptothecin (CPT). It is a hydrophobic drug that dissolves slightly in water and is used to treat lung, cervical and ovarian tumors [74]. The drawbacks of using TPT include the high toxicity of the carboxylate form and the weak cellular uptake. They were tackled by loading the drug in many nanocarriers, including MOFs, to control the release with high loading. These led to a decrease in toxicity and an increase the amount of TPT taken up by the cells [75].

TPT was loaded in porous Fe-MIL-100 to control the release with high loading capacity. The MOF was prepared by the hydrothermal method via microwave heating. A mixture of 8.97 mmol of iron(III) chloride and 4.02 mmol of trimesic acid [$C_6H_3(CO_2H)_3$] in 20 mL of demineralized water was heated to 130°C for 6 minutes under stirring, while applying 400 W of microwave power (to reduce the crystallization time). Then, the mixture was centrifuged for 10 min at 10,000*g to separate the nanoparticles. The particles were later washed with 50 mL of ethanol and recovered by centrifugation [75].

Aqueous solutions of the drug with 0.004, 0.04, 0.14, 0.42 and 2.05 mM concentrations were prepared. The loading was carried out by incubating 3 mg of the MIL-100 in 4.5 mL of the TPT solution and the mixture was divided in 3 microcentrifuge tubes of 1.5 mL. They were stirred for 24 h at room temperature and

the loaded nanoparticles were separated from the water by centrifugation for 10 min at 10,000*g. Then, they were washed 3 times with water and kept at 22 °C under vacuum for 24 h. A general scheme of the loading is shown in Figure 15 [75].

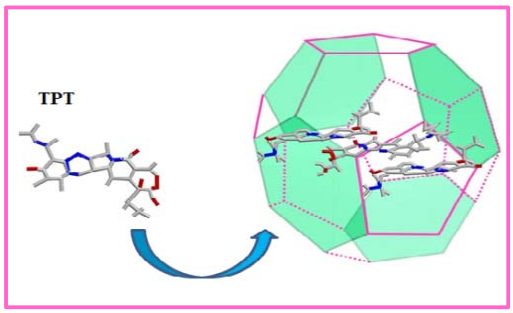


Figure 15: Scheme of entrapping TPT within MIL-100 nanoMOFs [75].

The percentages of the drug encapsulated in the MOFs by weight (mg encapsulated drug/mg nanoMIL-100) at the five concentrations were determined using ultraviolet (UV)-visible spectroscopy and found to be approximately 0.14, 1.3, 4.0, 5.6 and 33 wt.%, respectively. Another aqueous solution of the drug (0.023 mM) was prepared and the loading was achieved using seven successive impregnations. Two mg of MIL-100 were added to 9 mL of the drug solution and kept at room temperature for one day. After that, the loaded MOFs were centrifuged for 10 min at 10,000*g and washed with water. These steps were repeated seven times using fresh TPT solution in each impregnation and the resulting nanoparticles were kept at 22°C under vacuum for 24 h. The cumulative loading percentage after the last incubation was 11.6 wt.% [75].

For the highest loading, 33 wt.%, the transmission electron microscopy (TEM) technique confirmed that the nanoparticles had the same size distribution and structure before and after the drug encapsulation as shown in Figure 16. The diameter range of most of these nanocarriers varied between 50 and 150 nm, whereas few of them were larger (their sizes ranged between 200 and 400 nm). The release was investigated for different loading percentages (1.4, 11.6 and 33 wt.%) in two media (water at pH ~ 6.7 and PBS at pH ~ 7.4) at 37°C with and without photon irradiation. After 24 h of incubation in water, the fluorescence detected that 5.0 and 4.0 % of the drug was released from the first two loadings, respectively, whereas the highest loading (33 wt.%) did not show significant release (it was only 0.005%) [75].

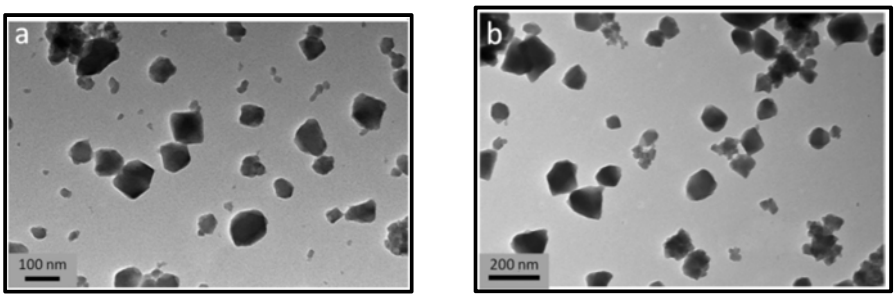


Figure 16: TEM of MIL-100 nanoMOFs (a) before and (b) after TPT encapsulation at 33 wt.% drug payload [75].

When one photon irradiation has been applied for the three payloads, the release was increased to 9.0, 13, and 2.5%, consecutively. In addition, two-photon irradiation was applied for 11.6 and 33 wt.% loadings and the corresponding release percentages were determined to be 28 and 2.8%. On the other hand, after 24 h of incubation in PBS, the lowest loading (1.4 wt.%) showed the fastest release. Around 60% of the loaded TPT was released within the first hour and 93% after 24 h [75]. The phenomenon of releasing higher amounts of the drug initially (that happened in the case of 1.4 wt.% payload) within a short period is called burst release which reduces the targeting of the drug to the tumor cells and increases the toxicity level [76]. The percentages of the release for 11.6 and 33 wt.% payloads were detected after 26 h of incubation and found to be around 40 and 15%, respectively [75].

The *in vitro* study of 11.6 wt.% loaded nanoMOFs was performed using human MiaPaCa-2 (lung carcinoma), PANC1 and A549 (pancreatic cancer) cells. Free TPT was incubated with the three cell lines for 72 h and $IC_{50}$ was found to be 0.4, 1.6 and greater than 25 μM for MiaPaCa-2, A549 and PANC1 [75], respectively, whereas the encapsulated drug showed different results (0.2, 2.5 and 2.4 μM). Results showed that using the loaded drug does not have significant effect on the antitumor activity in the case of MiaPaCa-2 and A549 compared to free TPT. In contrast, the loaded TPT showed remarkable improvement in the antitumor activity when it was used to treat the PANC1 cell line as these cells resisted the free TPT even at higher concentrations [75].

Busulfan is a chemotherapeutic agent used in high doses to chronic myelogenous leukemia [77] and used lately in the treatment of osteosarcoma [78]. The aim of encapsulating this drug in porous MOFs was to avoid its high degradation in aqueous solutions and prohibit its accumulation in the liver [79] by obtaining high

loading and controlling drug release. Four MOFs (MIL-88A, MIL-89, MIL-53 and MIL-100) were synthesized, then the drug was loaded in these MOFs through mixing and the release and loading were studied. MIL-88A was synthesized by heating 10 mL of iron chloride hexahydrate ($FeCl_3.6H_2O$) and 10 mmol/L of fumaric acid ($C_4H_4O_4$) while being mixed for two min at 80°C (with 600 W microwave power applied to assist in the heating). The second MOF (MIL-89) was obtained when 1 mmol of iron acetate ($C_{14}H_{27}Fe_3O_{18}$) was mixed with 1 mmol of trans,trans-muconic acid ($C_6H_6O_4$) and dissolved in 5 mL of methanol and 0.25 mL sodium hydroxide. The liquid mixture was heated for 6 hours in a Teflon-lined steel autoclave at 100°C [79].

The third MOF (MIL-53) was prepared solvothemally by heating a mixture of 1 mmol of $FeCl_3.6H_2O$ with 1 mmol of BDC [$C_6H_4(CO_2H)_2$] and 5 mL of DMF solvent at 150°C for 2 h. Finally, MIL-100 was obtained by mixing 8 mmol of aqueous iron ion, 5.3 mmol of BTC, 4 mmol of hydrogen fluoride and 40 mL of water. Then, the mixture was placed in a pressure chamber (autoclave) and heated under microwave irradiation for 30 min until it reached 200°C After that, the four mixtures were centrifuged for 10 min at 5,600*g and washed with 100 mL of deionized water to obtain MIL-88A and 100 mL of ethanol to obtain MIL-89, MIL-53 and MIL-100. Then they were centrifuged another time and dried at room temperature. MIL-88A and MIL-89 had faceted structures with sizes ranging between around 100 ± 25 and 75 ± 25 nm, respectively, whereas MIL-100 and MIL-53 represented trigonal shapes with mean diameters of 100 ± 50 and 350 ± 100 nm, respectively. The SEM and TEM of the four MOFs are presented in Figure 17 [79].

To carry out the loading of busulfan in the synthesized MOFs, two solutions of the drug were prepared using dichloromethane and acetonitrile solvents to obtain concentrations of 10 and 30 mg/mL, respectively. Then, 25 mg of the final MOFs produced were dehydrated at high temperatures, suspended in 2.5 mL of the busulfan solutions and stirred for 16 hours. Then, 25 mg of the final MOFs produced were dehydrated at high temperatures, suspended in 2.5 mL of the drug solutions and stirred for 16 hours [79]. The loaded particles were recovered by centrifugation for 10 min at 5,600*g and kept at room temperature under vacuum for 72 h. After that, 20 mg of MIL-53 and MIL-100 nanoparticles were incubated in 2 mL of the drug

solution (from 10 mg/ mL of busulfan solution in dichloromethane) and 1 µL of acetonitrile for 24 h at room temperature under stirring [79].

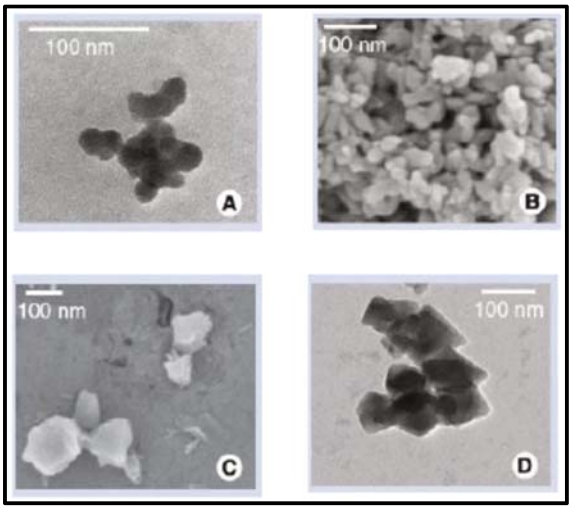


Figure 17: (A) MIL-88A (TEM); (B) MIL-89 (SEM); (C) MIL-53 (SEM) and (D) MIL-100 (TEM) [79].

The nanoparticles were separated using the same procedure mentioned above and the loading percentages were determined by nuclear magnetic resonance (NMR) spectroscopy and found to be around 13 and 25 wt.% (mg encapsulated drug/mg MOF) for MIL-53 and MIL-100, respectively. Another procedure for loading, namely elemental analysis, was implemented on the dried loaded nanoparticles for the four MOFs and the payloads were about 8, 14, 10 and 26 wt.% for MIL-88A MIL-53 MIL-89 MIL-100, respectively [79].

The release was investigated for MIL-100 and MIL-53 at pH 7.4 by suspending 25 mg of the encapsulated busulfan in PBS at 37°C under stirring for different periods of time and centrifugation at 5,600*g for 10 min. After each incubation, 1 mL of the solution was replaced with fresh PBS. The release of the encapsulated drug was 38% in the case of MIL-53 and 61% for MIL-100 during the first 30 minutes in PBS. After 2 h, the release increased to 58% and 76%, respectively, whereas the remaining portion was released within 6 h. Additionally, some *in vitro* experiments were carried out on human multiple myeloma (RPMI-8226), human leukemia (CCRF-CEM) and human macrophages (J774) cell lines to compare the cytotoxicity of free and loaded busulfan in MIL-100. After incubating them for 48 h, the loaded drug showed similar results of cytotoxicity compared with the free drug [79].

Another application of MOFs as anti-cancer drug carriers has been reported recently by loading DOX in MIL-100(Fe) [25]. DOX is a cytotoxic anti-cancer agent used frequently for childhood solid tumors, breast cancer, soft tissue sarcomas, myeloblastic leukemias and lymphomas [80]. Although it is used widely, it has adverse side effects including vomiting, nausea, hair loss, necrosis and oral mucositis, all of which limit its use [81]. The three main issues related to DOX's use in cancer treatment clinics are: cardiotoxicity during the first two or three days of use [82] which causes congestive heart failure and heart muscle disease (cardiomyopathy) [83], its tendency to self-assemble in aqueous solutions limiting the amount of the drug taken up by the cells, and the cancer cells resistance observed after a short therapy period [84].

To overcome the disadvantages of using DOX, it was loaded in MIL-100(Fe) which was synthesized by the same procedure mentioned in the case of loading TPT (6.0 mmol of iron(III) chloride was used instead of 8.97 mmol and the other amounts are the same). Five mg of the MOF were added to 1.5 mL of aqueous DOX (10 mg/mL) and stirred for 24 h. To increase the loading, the incubation was repeated twice and then the loaded particles were separated by centrifugation at 5,600*g for 15 min and left to dry for 3 days under vacuum. The loading was investigated by UV−visible spectroscopy and found to be 9.0 wt.% (mg encapsulated DOX/mg MIL-100 (Fe)). On the other hand, the release was studied using 5 mg of the encapsulated drug in 2 mL of PBS at pH 7.4. The drug release study showed fast release kinetics that reached 25% during the first 12 h, and then took a longer time to reach a complete release after 13.5 days. Figure 18 shows the structure of DOX-MIL-100(Fe) [25].

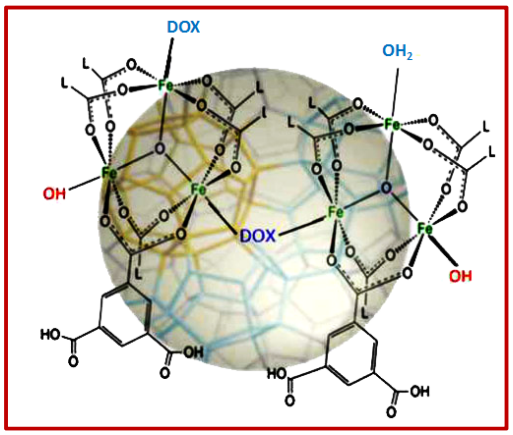


Figure 18: MIL-100(Fe) with DOX [25].

Zeolitic imidazole frameworks (ZIFs) are another example of MOFs synthesized using zinc salts and imidazole organic compounds and used in drug delivery. One compound that belongs to this category, ZIF-8, was synthesized by mixing 330 mg of 2-methyl imidazole ($C_4H_6N_2$) with 150 mg of zinc nitrate hexahydrate [$(Zn(NO_3)_2.6H_2O$] after dissolving each component in 7.15 mL of methanol in a glass container. Then, 0.15 mL of 2 mg/mL fluorescein (model drug) dissolved in methanol was added to the zinc precursor. The solution of 2-methyl imidazole was then poured into the zinc and fluorescein concoction and stirred for 5 min. The solution was milky indicating the progression of the reaction and hence the formation of the loaded nanoparticles [85].

The nanoparticles were separated from the solution by centrifugation at 7,000 rpm for 10 min and then washed three times with 10 mL of methanol to remove any remaining unreacted materials. The encapsulated fluorescein had a yellow color and was stored as a suspension in 5 mL methanol for further use. The resulting nanospheres had porous crystalline structure and their average size was measured to be 70 nm. Their sizes were identical to those measured before loading the fluorescein. Figure 19 shows the loading of fluorescein molecules in ZIF-8 [85].

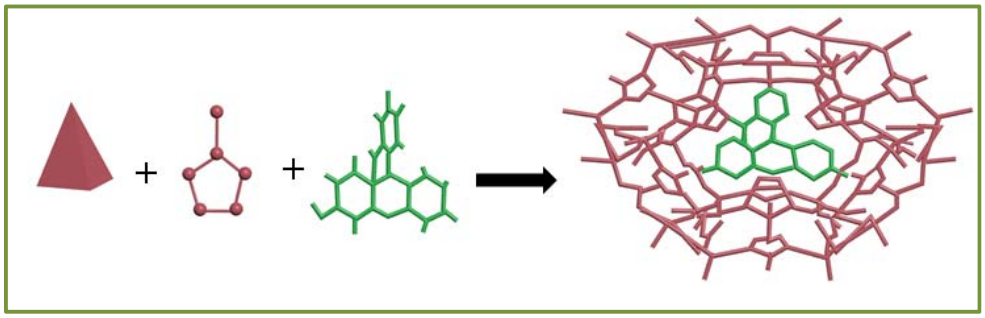

Figure 19: Fluorescein encapsulated inside of ZIF-8 frameworks [85].

Different amounts of fluorescein were loaded with a maximum loading of 1 wt.% (mg encapsulated fluorescein /mg MOF), which is comparable to the loading of other MOFs. Then, the stability of the nanoparticles was examined in PBS solution and their structures remained intact at neutral pH. The release was also measured using a fluorescence microscope and after 24 hours less than 10% of model drug was released. The low percentage of release was improved by lowering the pH (using an acidic buffer) and reached 50% after one hour. The loaded drug was then tested *in vitro* using MCF-7 breast cancer cells. The particles were capped with

cetyltrimethylammonium bromide (CTAB) and incubated with the cells for 12 hours. The half maximal effective concentration ($EC_{50}$) was measured to be 45 µg/mL, which is acceptable and comparable to the mesoporous silica nanomaterials and some other MOFs [85].

Camptothecin (CPT) - a chemotherapeutic agent- was loaded in ZIF-8 using the above mentioned procedure by adding 1 mg of the agent. As is the case with other anti-neoplastic agents, this drug was encapsulated in the MOFs to reduce its unwanted side effects. The loading of CPT molecules in ZIF-8 is shown in Figure 20 [85].

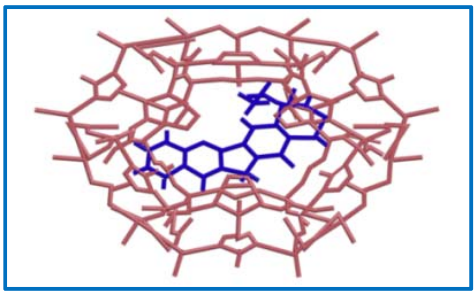

Figure 20: Camptothecin encapsulated inside of ZIF-8 frameworks [85].

The maximum loading obtained was 2 wt.% (mg encapsulated drug /mg MOF) and the $EC_{50}$ was found to be 22 µg/mL. After preparing the loaded drug, it was incubated with MCF-7 cells for 24 hours and the results showed that using CPT-ZIF-8 induced more cell death compared with those treated with free CPT. Additionally, it was shown that ZIF-8 better encapsulates molecules with negative charges, including camptothecin and fluorescein, and a lower of encapsulation was measured when positively charged molecules were used [85].

5-Fluorouracil (5-FU) is another anti-cancer drug that was loaded in ZIF-8 in an attempt to overcome its adverse effects [86]. It is used to treat various cancers including liver, breast, brain, gastrointestinal tract, pancreas and other solid tumors. The hematological, gastrointestinal and dermatological side effects of this cytotoxic drug limit its clinical applications, thus it was encapsulated in ZIF-8 to overcome these drawbacks [87]. The MOF was prepared by the procedure reported by Yaghi and co-workers [86]. Typical amounts of 0.21 g of $Zn(NO_3)_2.4H_2O$ and 0.06 g of 2-methyl imidazole were dissolved in 18 mL of DMF in a capped vial. The mixture was heated in a programmable oven gradually (at a rate of 5°C/min) to 140°C for 24 h followed by cooling (at a rate of 0.4°C/min) to room temperature. After that, the main

solution was removed and 20 mL of chloroform were added. The produced particles were collected, washed with 10 mL of DMF and left to dry in air for 10 min [88].

The drug loading study was performed by drying 20 mg of ZIF-8 in the oven at 160°C for 24 h and then stirring it with a solution of 5 mL of methanol containing 30 mg of 5-FU for 2 days. The resulting solution was dried at 50°C overnight and then the loading was determined by UV–visible absorption spectroscopy and found to be 0.66 g 5-FU/g ZIF-8. Furthermore, the release was measured at 37°C by a fluorescence spectrophotometer in two media, acetate buffer (pH 5.0) and PBS (pH 7.4). In PBS, 50% of the loaded 5-FU was released at the early stage (after around 10 h) and the remaining portion showed slow release which reached approximately 85% after 7 days [86].

The release increased remarkably in acetate buffer and reached more than 45% in 1 h, while only 17% was released in PBS within the same meantime. After 12 h, the release reached a plateau and 85% of the drug was released from the MOF. It was concluded that the rate of release from ZIF-8 is faster in acidic medium (tumor tissues) than during blood circulation (neutral pH environment). The SEM images of ZIF-8 immersed in different pH buffers are shown in Figure 21 [86].

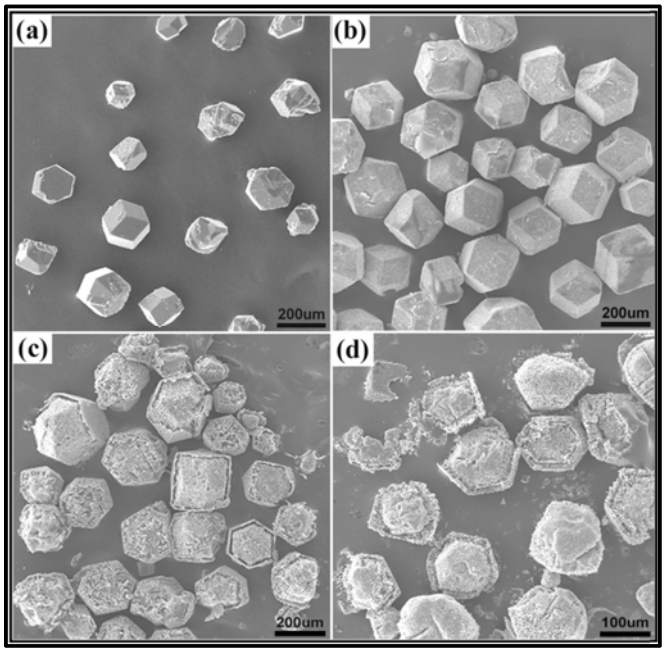


Figure 21: SEM images of ZIF-8 immersed in different pH buffers (pH 7.4 PBS and pH 5.0 acetate, respectively) for (a) 0 day (as-prepared); (b) 7 days in pH 7.4 buffer; (c) 5 minutes in pH 5.0 buffer and (d) 15 minutes in pH 5.0 buffer [86].

Moreover, DOX was incorporated in ZIF-8. The MOF was synthesized by mixing 0.6 g of zinc nitrate hexahydrate salt dissolved in 10 mL of methanol in a scintillation vial and 1.3 g of 2-methyl imidazole dissolved in 10 mL of methanol in another vial. The organic linker solution was added to the metal precursor and stirred for 30 min. Then, the nanospheres were centrifuged, washed 5 times with methanol, placed in an oven at 100°C to dry, and kept at room temperature to load the drug. ZIFs-8 and DOX are positively charged, so the procedure used to encapsulate fluorescein and camptothecin could not be followed and hence the researchers used another method to achieve a high loading percent. Two mL of 0.5 mM DOX methanol solution were mixed with 100 mg of ZIFs and stirred for 2 days. The DOX-ZIFs particles were collected by centrifugation, washed with methanol several times, dried and became ready for more experiments [89].

The percentage of DOX loaded inside the MOF was found to be 52% of the initial amount used in the preparation experiment. ZIF-8 is stable at neutral pH and starts to dissociate in acidic solutions, so the release was expected to occur as the cancer cells are acidic, whereas the pH of the normal cells is around 7.4 and at this pH value the release is very slow (the dissociation of ZIF-8 becomes difficult) which confirms that these cells will not be affected by the drug and remain intact. The release was measured for 2.5 h at pH 5, 6, and 7.4, and it was obvious that its rate decreased with increasing pH. Lowering the pH below 5 did not show any effect on the rate of release. This mechanism of DOX release is different from that reported in other drug delivery systems such as other MOFs [70] and silica [90]. A simple scheme representing the encapsulation of DOX into ZIF-8 is shown in Figure 22 [89].

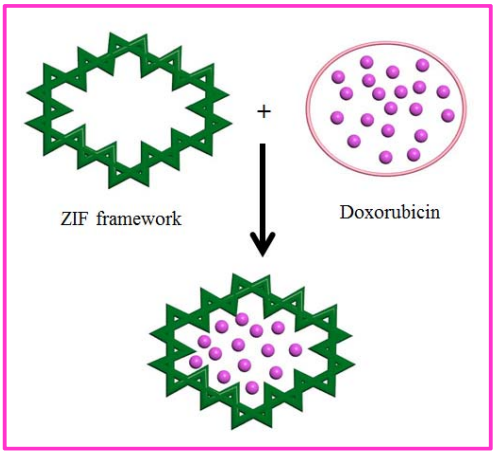


Figure 22: Encapsulation of DOX inside ZIF-8 framework [89].

Recently, Zheng *et al.* reported the encapsulation of a natural anti-neoplastic agent, namely curcumin (CCM), in ZIF-8 [91]. Several studies have shown that the anti-cancer activity of CCM would inhibit the proliferation and progression of many tumors including breast, pancreatic, colon, head and neck, prostate and many other types of cancer [92]. The main drawback of CCM is its incapability to be administrated in a systematic manner, because of its strong hydrophobic nature (poor absorption) and rapid metabolism [91, 93]. To overcome these shortcomings, several nanocarriers including silica nanoparticles [94], liposomes [95], micelles [96] and others were used to encapsulate CCM. However, the encapsulation procedure in these nanocarriers is complicated and requires relatively long time; thus a new attempt to deliver this anti-neoplastic agent was undertaken [91].

Zheng *et al.* developed a new strategy to load the CCM during the synthesis of ZIF-8 nanoparticles. A typical amount of 150 mg of zinc nitrate hexahydrate was dissolved in 5 mL of deionized water, whereas 5 mg of the drug and 330 mg of 2-methyl imidazole were dissolved in 10 mL of methanol. The two mixtures were stirred and after 1 min the solution became milky indicating the formation of the loaded nanoparticles (CCM@NZIF-8). The loaded nanoparticles were collected by centrifugation at 10,000 rpm for 15 min. Then, they were washed with 20 mL of methanol 3 times and stored as a suspension in 5 mL of methanol for further experiments. After drying the suspended particles, the reaction yield for a single synthesis was found to be 31 mg of CCM@NZIF-8 [91].

To find the CCM content, the dried nanoparticles were decomposed in 0.05 mL of 2 M HCl and the resulting solution was diluted to 2 mL by adding ethanol. The loading efficiency and capability were determined by analyzing the diluted mixture with an UV−visible spectrophotometer and calculated to be 88.2% (mg loaded drug/mg drug fed) and 12.7 wt.% (mg loaded drug/mg loaded nanoparticles), respectively. The average diameter of CCM@NZIF-8 is 119.3 ± 13.6 nm and their morphologies are shown in Figure 23 [91].

*In vitro* experiments were performed to study the release behavior of CCM as follows: 3 mg of CCM@NZIF-8 were added to 2 mL of PBS (pH 5.0 and 7.4) containing 1 wt.% Tween-80 in a dialysis bag. Then, the suspension was incubated in 8 mL of PBS solutions. In an acidic medium (pH 5.0), the release reached 43.4% in 2 days, while only 15.6% of the drug was released at neutral pH (in PBS) within the

same meantime. This result confirmed that the tumor acidic environment results in faster release of the drug from ZIF-8 in, which agrees with previous studies [86]. Furthermore, Zheng *et al.* measured the $EC_{50}$ for the ZIF-8 nanoparticles incubated with HeLa cells for 48 h and found it to be 63.8 μg/mL. This value is higher than that reported previously (45.0 μg/mL) for the same MOF [85]. On the other hand, the same cell line was incubated with CCM@NZIF-8 and CCM for 2 days. The encapsulated drug showed higher cytotoxicity ($IC_{50}$ = 3.0 μg/mL) compared to free CCM ($IC_{50}$ = 5.4 μg/mL) [91].

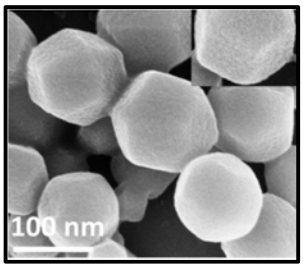


Figure 23: SEM image of CCM@NZIF-8 [91].

*In vivo* experiments were conducted on U14 cervical cancer xenograft in Kunming male mice. When the tumor size grew to an approximate size of 200 $mm^3$, the mice were divided into groups. They were injected 6 times every 2 days for 2 weeks with saline, free CCM (dissolved in a mixture of ethanol and cremophor eL and diluted with sterile saline) and CCM@NZIF-8. The dosage of CCM and CCM@NZIF-8 was 2.5 mg CCM / kg body weight. After two weeks, the tumors were resected and their weights were found to be 5.98 ± 1.39 g, 3.38 ± 0.9 g, and 0.9 ± 0.23 g, after treatment with saline, free CCM and CCM@NZIF-8, respectively, as shown in Figure 24. It was concluded that CCM@NZIF-8 had higher anti-cancer efficiency *in vivo* and *in vitro* compared to free CCM [91].

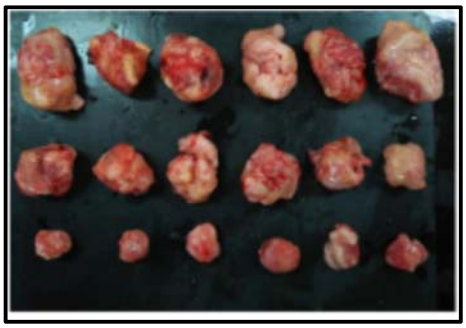

Figure 24: Photo of the excised tumors after 14 days of treatment by saline (top), free CCM (middle) and CCM@NZIF-8 (bottom) [91].

In 2016, Zhang *et al.* developed a new procedure called one pot synthesis to incorporate DOX in ZIF-8 with the aim of achieving a higher loading compared to the previously reported results [89]. First, an aqueous solution of zinc nitrate hexahydrate was prepared by dissolving 0.2 g of the metal salt in 0.8 g of water at pH 8. Four mL of DOX dissolved in deionized water at three concentrations (2, 6 and 10 mg/mL) were stirred with the metal precursor for 1 min. Then, 2 g of 2-methyl imidazole were dissolved in 8 g of deionized water and added gradually to the previous mixture [97].

The whole mixture was stirred for 15 min and the loaded particles (DOX@ZIF-8) were collected by centrifugation. They were washed 3 times with a mixture of water and methanol and dried under vacuum at ambient temperature [97]. The loading percentages were calculated using an UV-visible spectrophotometer and found to be 4.0, 14 and 20 wt.% (mg DOX/mg loaded ZIF-8) for the DOX concentrations of 2, 6 and 10 mg/mL, respectively. The sizes of the particles ranged 70−300 nm and their morphologies are shown by the SEM images in Figure 25 [97].

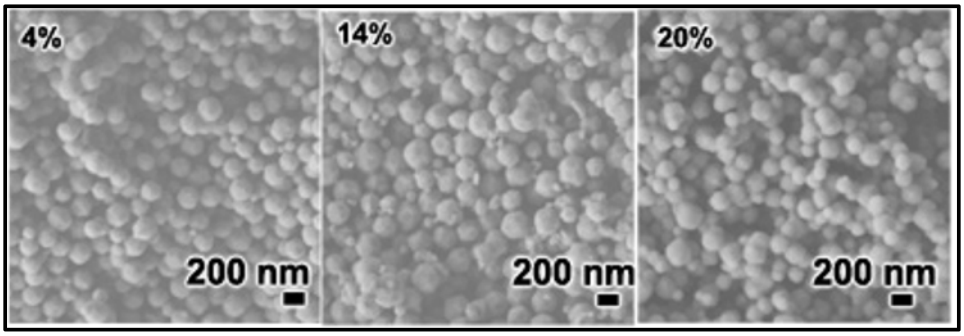


Figure 25: The SEM images of DOX@ZIF-8 particles with 4.0, 14 and 20% DOX loading [97].

The release study was carried out for 20 wt.% loaded ZIF-8 as follows: 10 mg of the dried particles were suspended in 20 mL of PBS containing 10 volume% of fetal bovine serum (FBS) at different pH values (4.0, 5.0, 6.0, 6.5 and 7.4) at 37°C under shaking at 150 rpm. At certain time points, 1 mL of the supernatant was taken and its fluorescence was measured using an UV-visible spectrophotometer and returned to the original release medium. There was no significant release detected after 15 days at pH ≥ 6.5, while 95% of the drug was released steadily at pH 5.0 and 6.0 during 7-9 days (the release increased by only 2% during this 2 days interval) [97].

In addition, the effect of the pH environment on the drug release was investigated using a different procedure. Typically, 10 mg of the loaded MOF were added to PBS containing 10 volume% of FBS and kept for a week. Then, some HCl drops (0.6 M) were added to adjust the pH to 6.5 and left for another week. Finally, the pH of the solution was adjusted to 6.0, 5.0 and 4.0 over 3 days. To determine the release behavior at each pH value, the same steps mentioned above were followed. The release was also insignificant at higher pH values (7.4 and 6.5) and increased remarkably to reach around 20, 70 and 100% at pH values of 6.0, 5.5 and 5.0, respectively [97].

The cytotoxicity values of free and encapsulated DOX were compared using several breast cancer cell lines (MCF-7, MDA-MB-231 and MDA-MB-468). The cell lines were treated with different doses of equivalent concentrations of DOX and DOX@ZIF-8 for 24 h and the results showed higher cytotoxicity of DOX@ZIF-8 compared to free DOX. When 0.1 μg/mL of DOX and 0.5 μg/mL of DOX@ZIF-8 were used, the percentages of the mitochondrial function decreased from its original value (100%) to 16, 20 and 43% in MDA-MB-231, MDA-MB-468 and MCF-7 cells, respectively. However, at lower concentrations, the loaded and free DOX showed only slight effect on the cells. At concentrations of 0.2 μg/mL of DOX and 1.0 μg/mL of DOX@ZIF-8, the percentages of the mitochondrial function decreased to below 10%. On the other hand, the mitochondrial function almost disappeared in the three cell lines when the incubation period was increased to 3 days [97].

DOX was encapsulated successfully in another MOF that was prepared from gadolinium (III) salt and 1,4-bis(5-carboxy-1H-benzimidazole-2-yl)benzene)) linker (pDBI) [98]. First, 0.02 g of pDBI were dissolved in 1.5 mL of DMF and added to 2.5 mL of $Gd(NO_3)_3.6H_2O$ solution (0.023 g). Then, the aqueous mixture was sonicated for 10 min in an ultrasound bath, heated at 110°C for 3 days in a closed vial and the crystals were collected. The synthesized Gd-pDBI (50 mg) was ground by a ball milling machine for 30 min to downsize the particles from 0.5 mm to 120 nm (to produce MG-Gd-pDBI) and then used to encapsulate DOX. The grinding did not affect the porosity and the crystalline structure of Gd-pDBI. Both MOFs (Gd-pDBI and MG-Gd-pDBI) had a rod-like shape as shown in Figure 26 [98].

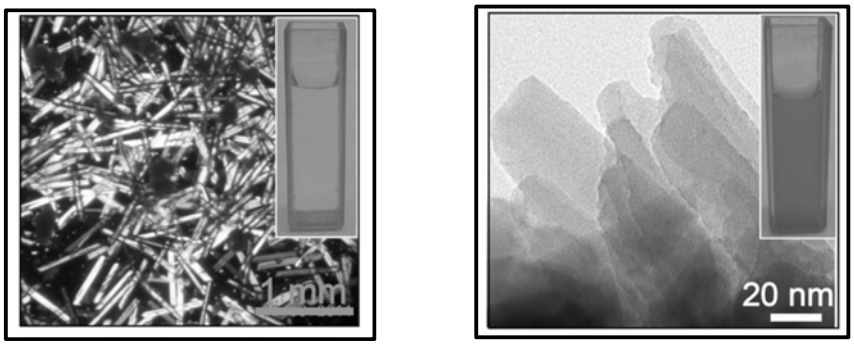


Figure 26: SEM images of Gd-pDBI (left) and MG-Gd-pDBI (right) [98].

The drug loading was performed as follows: the MOF particles were sonicated in 5 mL milli-Q (ultrapure) water. Then, 2 mg of DOX were dissolved in 1 mL milli-Q water, added to the MG-Gd-pDBI solution and sonicated for 5 min. The mixture was left under stirring in the dark for one day to get MG-Gd-pDBI- DOX. After that, the loaded particles were collected by centrifugation at 12,000 rpm for 15 min followed by washing twice with abundant milli-Q water. The DOX concentration was varied from 0.33 to 2 mg/mL and the loading was found to be 5 wt.% and 12 wt.% (mg encapsulated DOX/mg MG-Gd-pDBI), respectively [98].

The release behavior was studied in two different environments (pH 7.4 and 5) using 5 mg of the loaded drug in 3 mL of buffer solution. At pH 5, 44% of the DOX was released from 5 wt.% loaded particles in 5 days, whereas only 22% of the anti-neoplastic agent was released at neutral pH. This result insures that the effect of the anti-cancer drug on healthy cells will be less pronounced compared to its effect on cancerous tissue, and hence the side effects will decrease. Both *in vitro* and *in vivo* experiments were conducted to measure the efficiency of MG-Gd-pDBI-DOX as a drug delivery system (DDS). A model cell line (namely U 937 which is a human leukemia cancer cell line) was incubated for 2 days with the MOF to examine the *in vitro* anti-cancer activity and 50% of the cancer cells were inhibited at a DOX concentration of 75 mg/mL [98].

Further experiments were carried out and confirmed that the MG-Gd-pDBI is stable and biocompatible in blood plasma. Also, they showed that every Gd-linker contained two DMF molecules which are undesirable [98], because the DMF is toxic and may precipitate in the liver [99]. Another set of experiments were conducted to evaluate *in vivo* toxicity of MG-Gd-pDBI on healthy young (8 weeks old) Swiss albino mice that weighed about 20-22 g. Under the same conditions, it was observed

that mice injected with suspended MG-Gd-pDBI in water did not show any serious health problems or an increase in mortality rate [98].

Moreover, the blood and serum biochemical components were not affected by the MOFs and their values were the same as for the non-injected mice. Also, the kidney regulators and other parameter including the total phosphorous and protein contents remained unchanged. The functions of the other organs including heart, brain, spleen and lung were not affected in both treated and normal murine and the only minor health deterioration was found in the liver whereas some of the MG-Gd-pDBI has accumulated. The study concluded that encapsulating DOX in MG-Gd-pDBI was feasible and could lead to designing a new DDS based on MOFs [98].

A new efficient strategy was developed to target therapies by magnetic MOFs. MOFs that exhibit magnetic characteristics can be utilized to target the drug to the desired location by applying an external magnetic field source [100]. This method is applicable in the treatment of tumors with a known location [101]. Nimesulide (NIM) an anti-cancer agent, used in the treating of pancreatic [100], colorectal, breast, prostate and other tumors [102], was encapsulated in a three dimensional magnetic MOF [100], to reduce its adverse side effects (gastrointestinal intolerance and ulcers) [103]. The MOF was fabricated using iron oxide ($Fe_3O_4$) and $Cu_3(BTC)_2$ [100].

First, iron oxide magnetic nanoparticles were synthesized using the procedure reported by Mikhaylova *et al.* [104]. Typical amounts of 2.7 g (10 mmol) of ferrous sulfate ($FeSO_4.7H_2O$) and 2.7 g (10 mmol) of ferric trichloride ($FeCl_3.6H_2O$) were dissolved in 60 mL of distilled water. Drops of ammonia solution ($NH_3.H_2O$, 25%) were added and the mixture was stirred at 30°C. Then, the temperature was increased to 80°C for 30 min and $Fe_3O_4$ nanorods formed and precipitated. The particles were separated by centrifugation, washed 3 times with 30 mL of distilled water and dispersed in ethanol. After the evaporation of ethanol, the concentration of the resulting iron oxide particles was measured at approximately 7 mg/mL [100].

After obtaining $Fe_3O_4$ nanorods, 0.5 g (2.38 mmol) of BTC was dissolved in 80 mL of an equimolar mixture of ethanol and DMF. Then, 10 mL and 5 mL of ethanol containing $Fe_3O_4$ particles were added to the BTC mixture, stirred and heated to 70°C to obtain nanocomposites (1) and (2), respectively. Forty mL of copper (II) acetate (0.86 g, 4.31 mmol) aqueous solution was stirred with the mixture at the same temperature for 4 h. The final MOF particles were obtained by centrifugation, washed

once with 50 mL of water and three times with 10 mL of ethanol. Figure 27 represents the SEM images of nanocomposites (1) and (2) [100]. The two nanocomposites have mainly irregular shapes and their sizes ranging between 50 and 150 nm [100].

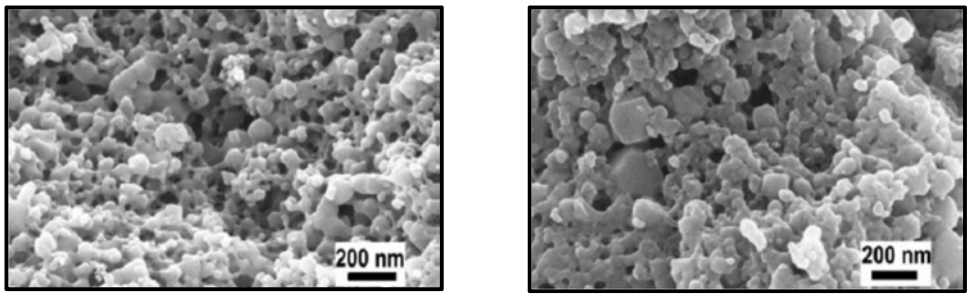


Figure 27: SEM images of nanocomposites (1) (left) and (2) (right) [100].

Before starting the loading, 800 mg of NIM were dissolved in 10 mL of trichloromethane. Then, 100 mg of the MOF were added to the mixture and stirred in a sealed vessel for 24 h at room temperature. The mixture was filtered, washed twice with 5 ml of trichloromethane and dried at 70°C under vacuum. UV-vis spectroscopy was used to determine the amount of NIM encapsulated in the pores of the magnetic MOF and found to be 0.172 and 0.201 g of NIM per gram of composites (1) and (2), respectively, which are comparable with the loading of drugs in other MOFs [100].

Release experiments were then conducted at 37 ± 0.2°C for nanocomposite (1). The loaded particles (100 mg) were suspended in 100 mL of physiological saline and the mixture was stirred. Five mL were removed at certain intervals of time for analysis by UV-visible spectroscopy and the same volume was replenished using fresh saline [100]. The release profile followed mainly three patterns. At the beginning, the release was rapid and approximately 20% occurred during the first 4 h (diffusion and dissolution of drug in aqueous medium). Then, it showed slow kinetics and 70% of the drug release took place within 7 days (desorption, diffusion and dissociation of drug from the framework pores to the aqueous solution). Finally, the remaining percentage (10%) was released very slowly taking approximately 4 days [100]. This slow phase of release is attributed to the interaction between the drug molecules and the unsaturated bonds in the framework [105].

More recently, amorphous MOF (UiO-66) based on zirconium (Zr) has been synthesized and used to encapsulate calcein. Calcein is a hydrophilic model drug mimicking the anti-neoplastic agent doxorubicin. It is used widely to study the drug encapsulation and delivery from nanocarriers [106]. The toxicity of Zr is low and it is

naturally found in the human body (at approximately 300 mg). Amorphous MOFs have disordered network structures; however, they have the original metal-ligand connectivity of the crystalline framework. UiO-66 was achieved by dissolving 125 mg of zirconium(IV) chloride ($ZrCl_4$) in 1 mL of HCl and 5 mL of DMF, whereas 123 mg of BDC were dissolved in 10 mL of DMF. The whole solution was placed in a Teflon autoclave and heated at 80°C for 16 h. After that, the resulting mixture was centrifuged at 5,500 rpm for 10 min and the collected particles were washed 3 times with ethanol and DMF. To remove the remaining solvents, the resulting white product was dried at 90°C under vacuum in an oven [107].

The loading was performed by stirring 20 mg of UiO-66 with 5 mL of methanol calcein solution at 37°C for 6 days. To separate the loaded drug, the mixture was centrifuged at 5,500 rpm for 20 min and washed twice with methanol. Then, it was centrifuged again for 10 min and dried overnight at 37°C. The amount of calcein loaded was measured by the TGA and found to be 4.9 ± 0.2 wt.% (mg calcein added/mg loaded UiO-66). About 0.2 g of the loaded particles were placed in a stainless steel jar in a Retsch MM200 mill and ground at 20 Hz using 8 mm stainless steel ball for 30 min to obtain amorphous loaded MOF. The particles sizes of loaded UiO-66 and amorphous UiO-66 were 261 ± 12 and 272 ± 157 nm, respectively. Figure 28 represents the SEM images of UiO-66 (left) and amorphous UiO-66 (right) [107].

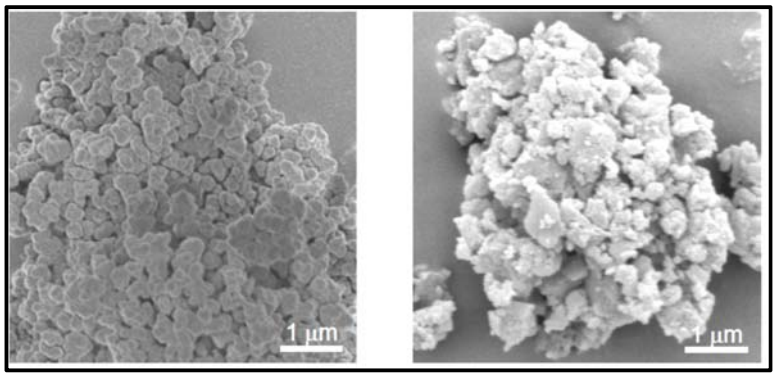


Figure 28: SEM images of UiO-66 (left) and amorphous UiO-66 (right) [107].

Calcein release (from UiO-66 and amorphous UiO-66) experiments were conducted by stirring 3 mg of nanocarriers with 1 mL PBS (pH 7.4) in an incubator at 37°C. The maximum release of calcein from UiO-66 was 97.07 wt.% and achieved within 2 days (half of this amount was released after 1.86 h). Furthermore, the release

from the amorphous UiO-66 was studied and showed two different kinetic rates. About 58% of the calcein was released by desorption and diffusion from the MOF (half of this amount was released after 14 h). After 10 days, a significant amount of calcein was found inside the amorphous UiO-66 nanocarriers and the release kinetics shifted to a very slow phase. The maximum release was reached after 30 days and found to be approximately 80%. The main disadvantage of using amorphous UiO-66 in this drug delivery system is that it showed the longest release reported from MOFs [107].

To investigate the cytotoxicity of empty UiO-66, *in vitro* studies were carried out on HeLa cells. $IC_{50}$ was measured after 24 and 48 h of incubation of the cells with the MOF and the values were found to be 1.503 ± 0.154 mg/mL and 1.357 ± 0.088 mg/mL, respectively, which are similar to the $IC_{50}$ reported for the Fe-MIL family. On the other hand, the same cell line (HeLa cells) was incubated with free calcein, loaded UiO-66 and amorphous UiO-66 for 24 h to determine the cellular uptake. The internalization efficiency was found to be very high in the case of both loaded MOFs, compared to the free model drug (because of its hydrophilic nature) [107].

The examples detailed above show the promise of using MOFs as drug delivery vehicles in cancer treatment.

# Chapter 3. Materials and Methods

In this chapter, the chemicals and methods used to prepare and characterize the MOFs are explained. Also, the results of the loading and release experiments are introduced and discussed.

## 3.1. Synthesis of MOFs

All chemicals were used as purchased from LABCO (the official Sigma-Aldrich distributor in the United Arab Emirates) without further modifications or purifications. For comparison purposes, the MOFs were synthesized using two synthesis routes: (1) by means of microwave irradiation and (2) solvothermally using a conventional electrical oven. The synthesis procedure was as the follows: iron nitrate nonahydrate ($Fe(NO_3)_3.9H_2O$, ACS reagent, ≥98%) and 2,6 naphthalenedicarboxylic acid (2,6 NDC, 99%) were dissolved in N,N-dimethylformamide (DMF, ReagentPlus®, ≥99%). The advantages of using the microwave technique utilized in this work include: short reaction times, uniform heating and a higher possibility to prepare crystals with smaller particles size [108]. Solvothermal technique is usually used because of its simplicity and the ability of controlling the morphology of these crystalline particles [109].

Typical amounts of 0.2307 mmol (93.2 mg) of iron(III) nitrate nonahydrate, 0.2307 mmol (49.9 mg) of 2,6 NDC and 10 mL of DMF were stirred using a magnetic stirrer (model HS15 from Misung Scientific Co., Ltd., Korea) at a speed of 5 rps for 5 min. Then, the solution was poured in a 23 mL Teflon autoclave bomb calorimeter (model 4781 microwave digestion bomb from Parr Instrument Company, USA) and heated in a microwave oven (model RCMT5088W from Frigidaire Company, USA) at 160 W for 5 min. To separate the produced particles (Fe-NDC-M), the resulting mixture was centrifuged (centurion scientific centrifuge, model EB Series, UK) at 5,500 rpm for 30 min. After that, the supernatant was removed and the pale yellow particles were washed twice with 5 mL of DMF to remove the unreacted materials. Finally, the collected MOF particles were dried in an electrical oven (Incubator Classic.Line with natural convection model BD 23 from BINDER GmbH Company, Germany) at 100°C for 1.5 h to evaporate all of the DMF.

The same batch composition as that utilized in the microwave technique (described above) was used to prepare the oven samples (Fe-NDC-O). The samples

were heated in the oven at 100°C for 24 h (instead of using a microwave as done for the first MOF). The remaining steps were carried out as described above.

### 3.2. Characterization Techniques

The resulting MOFs samples were characterized using X-ray diffraction (XRD), scanning electron microscopy (SEM), energy-dispersive X-ray (EDS) and Fourier transform infrared spectroscopy (FTIR) analytical techniques to determine their morphological features. These techniques are effective in determining the crystalline structure, size and composition of MOFs [110].

The XRD results were recorded from a conventional high resolution Bruker D8 Advance diffractometer (University of Sharjah) using a Cu Ka (k = 1.54 Å) radiation source on silicon wafer from 3 to 40º ($2\theta$) with a step size of 0.02º and 1 s (per step) in a continuous mode. In order to get the SEM image of Fe-NDC-M, the sample was coated with gold in a SC7620 mini sputter coater with a carbon fiber evaporation attachment (Quorum Technologies Ltd., UK) to make it electrically conductive and then a scanning electron microscope (model VEGA III LMU with Oxford X-Act EDS, Tescan Orsay Holding Company, Czech Republic) was used. For Fe-NDC-O, another model (VEGA III XMU with Oxford X-Max 50 EDS) from the same company was used (University of Sharjah). Before starting the analysis, samples were coated with carbon using the same coater mentioned above.

The Energy-dispersive X-ray (EDS) quantitative analysis for both MOFs was performed at two different positions of the sample as follows: a small amount of the sample was placed in an aluminum stub inside a scanning electron microscope (VEGA III XMU with Oxford X-Max 50 EDS) and the results were collected using the Aztec software. Despite the limitation of EDS analysis in detecting light elements (such as hydrogen), it can still be used as a characterization technique [111]. Finally, Spectrum one FT-IR spectrometer (Perkin Elmer Company, USA) was used to get the FTIR patterns. First, tiny amounts of the MOFs were added to 200 mg of potassium bromide (FT-IR grade, ≥99% trace metals basis from Sigma-Aldrich Company) and ground manually. Then, they were compressed by applying 3,000 tons uniaxial pressure and the resulting discs were placed inside the spectrometer to obtain the FTIR patterns. The results were recorded using spectra software.

### 3.3. Loading Experiments of the Model Drug

Calcein disodium salt (purchased from Sigma-Aldrich Company and used as received without purification) was loaded in the previously prepared MOFs. This model drug was selected for purposes of this research because it is fluorescent and thus can be detected by fluorescence spectroscopy. Also, it is cheaper and has a similar structure to the chemotherapeutic agent doxorubicin [107, 112]. The loading was carried out in two steps. First, 100 mg of calcein disodium salt were dissolved in 10 mL of neutral PBS to obtain a 15 mM solution. Some drops of HCl/NaOH were added carefully to maintain the pH at 7.4 (because it was observed that the pH values changed when calcein salt was added). Then, 130 mg of the dried MOFs were stirred with the model drug solution for 48 h at 5 rps. The resulting mixture was centrifuged at 5,500 rpm for 30 min and the collected loaded particles were dried in an oven at 100°C for 1 h.

To determine the loading efficiency (amount of model drug encapsulated/amount of model drug fed) [91], the fluorescence values of: (1) 50 µL of 15 mM calcein disodium salt solution diluted in 3 mL of PBS, and (2) 50 µL of the supernatant (after the loading) diluted in 3 mL of PBS, were detected by a fluorescence spectroscopy (QuantaMaster QM 30, Photon Technology International, USA) connected to FelixGX software with the emission wavelength set between 490 and 515 nm. The solutions were diluted because of the self-quenching (decrease in the fluorescence intensity) of calcein at high concentrations [113]. The loading experiments were repeated three times and the loading efficiencies were calculated using equation (1).

$$Loading\ efficiency\ \% = \frac{F_1 - F_2}{F_1} * 100\% \quad (1)$$

where,

$F_1$ = the fluorescence of the model drug solution (before the loading).

$F_2$ = the fluorescence of the supernatant after the loading.

### 3.4. Release Experiments of the Model Drug

The release kinetics of the model drug without ultrasound (from both encapsulated MOFs; microwave-prepared and oven-prepared) were studied. In addition, the effect of ultrasound irradiation on the model drug release percent was

investigated. The experiments were carried out as discussed in the following paragraphs (each experiment was repeated 4 times).

**3.4.1. Release from loaded Fe-NDC-M and Fe-NDC-O at 37 ± 0.5 °C without US.** Five mL of PBS were added to 3 mg of the loaded MOF. The fluorescence of the baseline (at time 0) was measured using the fluorescence spectroscopy after diluting 100 μL of the supernatant in 2 ml of fresh PBS. The remaining mixture was placed in a water bath at 37 ± 0.5 °C. The fluorescence values of 100 μL of the supernatant diluted in 2 ml of PBS were measured after 2, 4, 6, 8 and 10 min.

*Note: the concentrations of the main mixture decreased as 100 μL were taken to measure the fluorescence at each time point; therefore the fluorescence readings were corrected. This was done for all of the release experiments.

**3.4.2. Release from loaded Fe-NDC-M and Fe-NDC-O at 37 ± 0.5 °C after exposure to 40-kHz US.** Five mL of PBS were added to 3 mg of the calcein encapsulating MOF. The fluorescence of the baseline (at time 0) was measured after diluting 100 μL of the supernatant in 2 ml of PBS. The remaining mixture was exposed to 40-kHz US using a sonication bath (model DSC-50TH, Sonicor Inc., USA) for 2 min at 37 ± 0.5 °C. The fluorescence of 100 μL (of the supernatant diluted in 2 ml of fresh PBS) were measured after 2, 4, 6, 8 and 10 min.

**3.4.3. Release from loaded Fe-NDC-M and Fe-NDC-O at 37 ± 0.5 °C without US and after vorexing.** Five mL of PBS were added to 3 mg of the loaded MOF. The fluorescence of the baseline (at time 0) was measured after diluting 100 μL of the supernatant in 2 ml of fresh PBS. The remaining mixture was left in a water bath at 37 ± 0.5 °C for 2 min. Then, it was vortexed at 1,000 rpm for 10 s using a vortexing unit (Heathrow Scientific®LLC, USA) and centrifuged at 5,500 rpm for 5 min. Then, the fluorescence of 100 μL of the supernatant, diluted in 2 ml of fresh PBS, was measured. The remaining mixture was then vortexed at 1,000 rpm for 10 s (as some of the particles stuck on the wall of centrifuge tube). The same steps were repeated and the fluorescence values were measured after 4, 6, 8 and 10 min.

**3.4.4. Release from loaded Fe-NDC-M and Fe-NDC-O at 37 ± 0.5 °C after exposure to 40-kHz US and vortexing.** Five mL of PBS were added to 3 mg of the loaded MOF. The fluorescence of the baseline (at time 0) was measured after diluting 100 μL of the supernatant in 2 ml of fresh PBS. The remaining mixture was sonicated in the sonication bath at 37 ± 0.5 °C for 2 min. Then, it was vortexed at 1,000 rpm for 10 s using the vortexer and centrifuged at 5,500 rpm for 5 min. Then, the fluorescence of 100 μL of the supernatant diluted in 2 ml of PBS was measured, and the remaining mixture was vortexed at 1,000 rpm for 10 s. The same steps were repeated and the fluorescence values were measured after 4, 6, 8 and 10 min.

**3.4.5. Release from loaded Fe-NDC-M at room temperature without US.** Five mL of PBS were added to 6 mg of the loaded Fe-NDC-M. The fluorescence of the baseline (at time 0) was measured using fluorescence spectroscopy after diluting 100 μL of the supernatant in 2 ml of fresh PBS. Then, the mixture was left at room temperature and the fluorescence values of 100 μL of the supernatant diluted in 2 ml of fresh PBS were measured after 2, 4, 6, 8 and 10 min.

**3.4.6. Release from loaded Fe-NDC-M at room temperature after exposure to 20-kHz US.** Five mL of PBS were added to 6 mg of the MOF. The fluorescence of the baselines (at time 0) was measured. Then, the sample was immersed in a 200 mL of distilled water bath and exposed to 20-kHz US **(**20 s on and 10 s off**)** using an ultrasonic probe (model CV334 with coupler model 630-0421, Sonics & Materials, Inc., USA). The fluorescence was measured for 100 μL of the supernatant diluted in 2 mL after 2, 4, 6, 8 and 10 min.

**3.4.7. Maximum release.** To determine the maximum release, one of the samples used in the release experiments without US at 37°C and after exposure to 20-kHz US at room temperature were stirred at 1 rps for one week and then the fluorescence of 100 μL of the supernatant diluted in 2 mL was measured. These values were used to calculate the release percent for the experiments described above using equation (2).

$$Drug\ release\ \% = \frac{F_t - F_0}{F_{max} - F_0} \qquad (2)$$

where,

$F_t$ = the fluorescence at each time point.

$F_0$ = the fluorescence of the baseline (at t=0).

$F_{max}$ = the fluorescence achieved after a week of stirring.

### 3.5. Calculations and Statistical Analysis

The release percentages and standard deviations were calculated using Microsoft Excel (version 2010). The pairwise comparisons of the release percentages were performed using Tukey Kramer statistical test (a single-step multiple comparison method). The procedure and spreadsheet of this test are available online (http://udel.edu/~mcdonald/statanovasig.html).

### 3.6. Determination of the Power Density

The power densities of the probe (at room temperature) and the sonication bath (at room temperature and 37°C) were determined using a calibrated hydrophone (model 8103, Bruel and Kjaer Engineering Company, Denmark). Data of the acoustic spectrum (hydrophone responses, $V_{rms}$) were recorded using a digital storage oscilloscope (model TDS2002B, Tektronix Inc., USA). Then, equation (3) was used to calculate the power density [114]. It is derived using equations (4-13) listed below.

$$\bar{I} = \frac{\bar{V}_{rms}^2 \, Q}{Z} \tag{3}$$

where,

$\bar{I}$ = the average acoustic intensity.

$\bar{V}_{rms}$ = the root-mean-squared voltage of the hydrophone signal.

$Q$ = the frequency-dependent calibration factor obtained from the manufacturer that relates pressure to voltage.

$Z$ = the acoustic impedance ($Z$ for water = $1.5 \times 10^6$ kg/m$^2$s).

- Derivation of equation (3):

$$\text{dB (decibel)} = 10 \log (I/I_{ref}) \tag{4}$$

$$\text{dB} = 20 \log (V/V_{ref}) \tag{5}$$

$$\text{dB} = 20 \log (P/P_{ref}) \tag{6}$$

where,

V= voltage.

P = acoustic pressure.

The basic definition is: $dB = 20 \log_{10} (V/1V/\mu Pa)$ (7)

The voltage sensitivity of the hydrophone = -211 dB (from the manufacturer).

(-211/20) dB = -10.55 = $\log_{10}$ (V/1V/µPa).

V/1V/µPa = $10^{-10.55}$ = 2.8184 * $10^{-11}$ V/ µPa.

2.8184 * $10^{-11}$ (V/ µPa) * $10^{6}$ (µPa/1 Pa) * $10^{6}$ (µV/1V) = 28.184 µV/Pa.

28.184 µV/Pa = 28.184 * $10^{-6}$ V/Pa.

$$\bar{I} = \frac{\bar{p}^2}{Z_{water}} = \frac{\left(\sqrt{\bar{p}^2}\right)^2}{Z_{water}} = \frac{\left(\sqrt{\bar{V}^2\left(\frac{Pa^2}{(28.184 * 10^{-6}V)^2}\right)}\right)^2}{Z_{water}} \quad (8)$$

$$\bar{V}_{rms} = \sqrt{\bar{V}^2} \quad (9)$$

$$\bar{I} = \frac{\frac{Pa^2}{(28.184 * 10^{-6}\,V)^2}}{1.5 * 10^{6}\,\frac{kg}{m^2 s}} \bar{V}_{rms}^2 \approx \left(839.27 \frac{W/m^2}{V^2}\right).\bar{V}_{rms}^2 \quad (10)$$

$$\bar{I} \approx \left(0.0839\ \frac{W/cm^2}{V^2}\right).\bar{V}_{rms}^2 \quad (11)$$

- At 40 kHz:

Efficiency (from the manufacturer) = -3.2 dB.

Correction = $10^{(-3.2\ dB/10\ dB)} \approx 0.479$

$$\bar{I} \approx \left(0.0839 \frac{W/cm^2}{V^2}\right) * \frac{1}{0.479} \bar{V}_{rms}^2 \approx \left(0.1752\ \frac{W/cm^2}{V^2}\right).\bar{V}_{rms}^2 \quad (12)$$

- At 20 kHz:

Efficiency (from the manufacturer) = 0 dB.

Correction = $10^{(-0\ dB/10\ dB)} = 1$.

$$\bar{I} \approx \left(0.0839\ \frac{W/cm^2}{V^2}\right).\bar{V}_{rms}^2 \quad (13)$$

# Chapter 4. Results and Discussion

The results of the characterization analytical techniques, loading and release experiments are discussed in this chapter.

## 4.1. XRD Results

The XRD patterns of Fe-NDC-M and Fe-NDC-O are represented in Figure 29. The sharp peaks confirmed that the synthesized MOFs have crystalline structures. On the other hand, the angles ($2\theta$) of the sharp diffraction peaks for the two MOFs are similar, which means that their crystal sizes are in the same range.

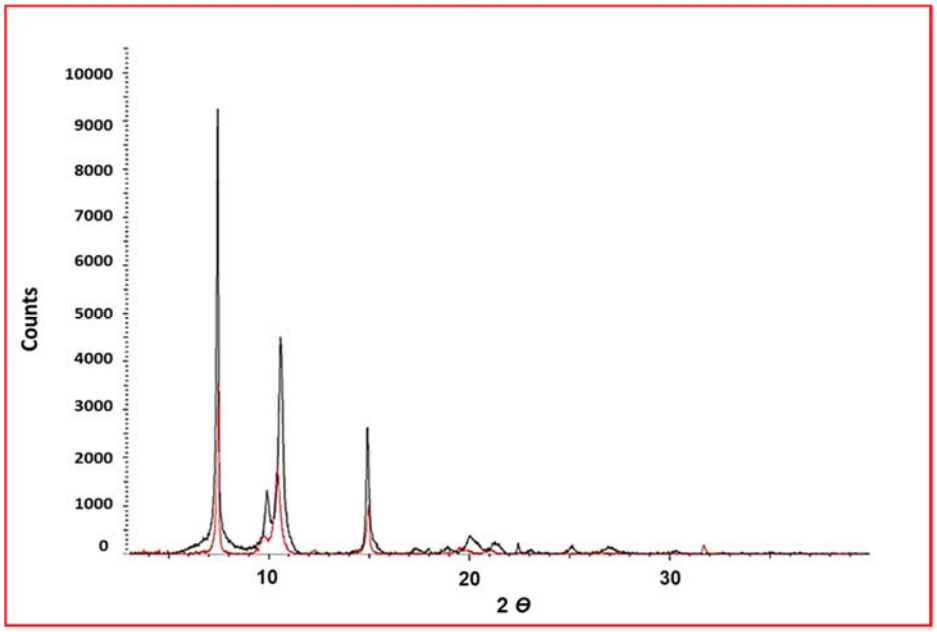


Figure 29: XRD of Fe-NDC-M (red peaks) and Fe-NDC-O (black peaks).

## 4.2. SEM Images

Figure 30 depicts the SEM images of the two MOFs. It was difficult to get a clear image for Fe-NDC-M (it requires a high resolution transmission electron microscopy (TEM) which is not available at AUS or UoS). The particles seemed to have a rod-like shape with a size in the nano range. The other MOF, Fe-NDC-O, was found to have a rod-like shape with a diameter ranging between 100-150 nm and a length of 400-600 nm. Many studies showed that rod nanoparticles including PEG-hydrogel rods (with aspect ratio of 150 × 450 nm), trastuzumab-coated nanoparticles

(367 ± 33 nm in length and 126 ± 8 nm in width) and others can target several cancer cell lines effectively, compared to other crystalline geometries [115, 116].

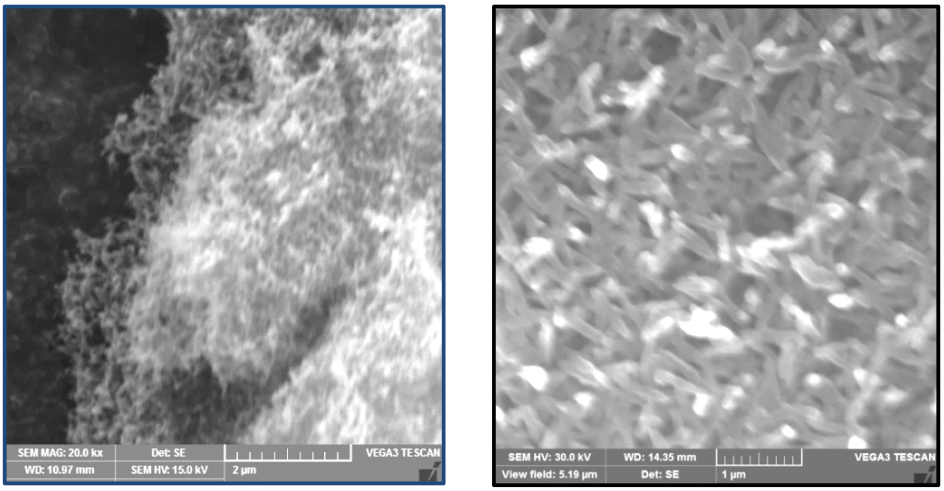


Figure 30: SEM images of Fe-NDC-M (left) and Fe-NDC-O (right).

### 4.3. EDS Results

The EDS patterns at two different positions for Fe-NDC-M and Fe-NDC-O are shown in Figures 31, 32, 33 and 34, respectively. The results confirmed the successful synthesis of both MOFs [117]. There is a small amount of aluminum present in Figure 31 (due to the aluminum stub on which the sample was placed). The difference between the composition wt.% at the two positions was very small, which confirms the preparation reproducibility of the two MOFs.

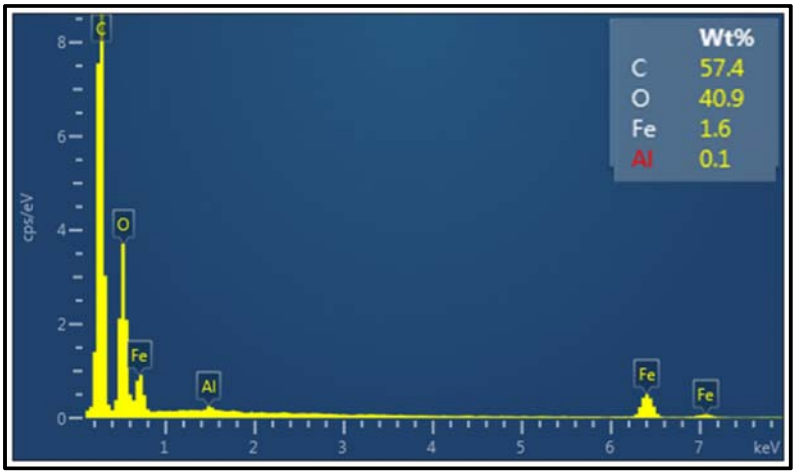


Figure 31: Elemental analysis of Fe-NDC-M at the first position.

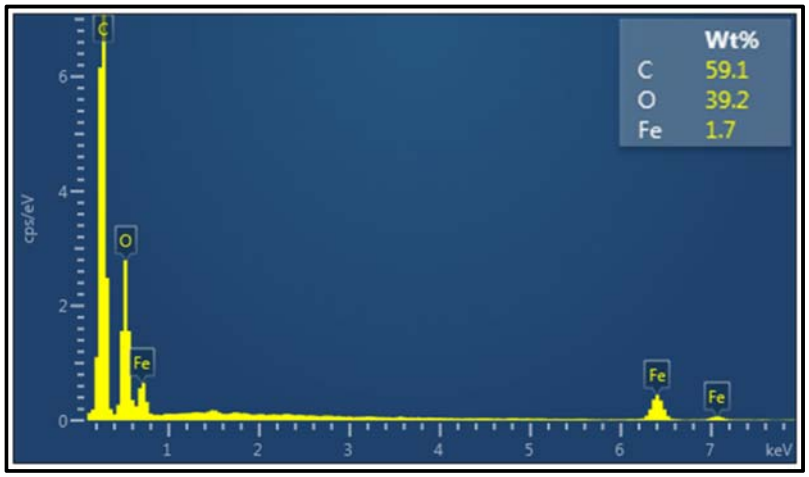


Figure 32: Elemental analysis of Fe-NDC-M at the second position.

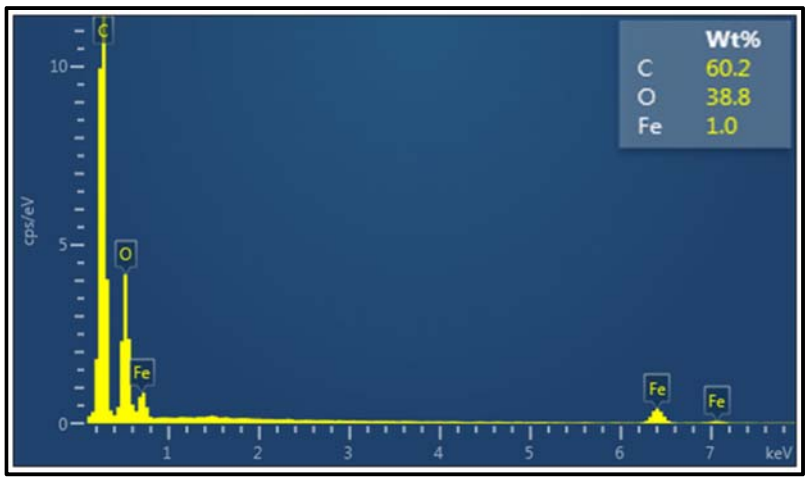


Figure 33: Elemental analysis of Fe-NDC-O at the first position.

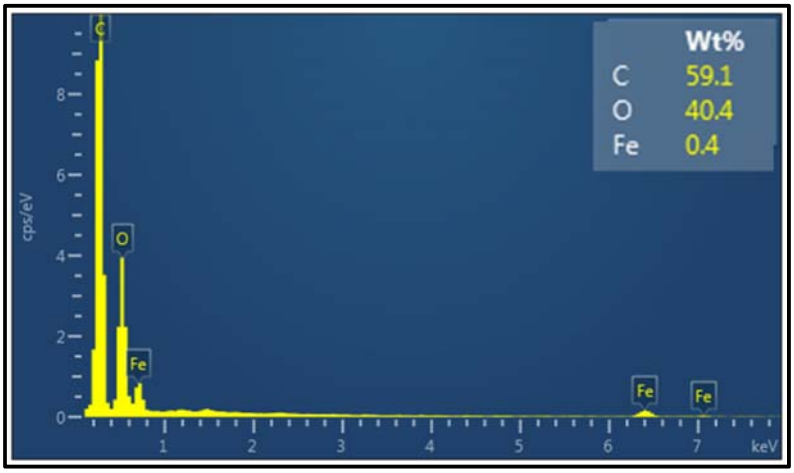


Figure 34: Elemental analysis of Fe-NDC-O at the second position.

## 4.4. FTIR Patterns

The FTIR patterns are presented in Figure 35. It was found that the absorption peaks of both MOFs were almost the same. In other words, the stretching and bending of the covalent bonds in molecules were similar in Fe-NDC-M and Fe-NDC-O.

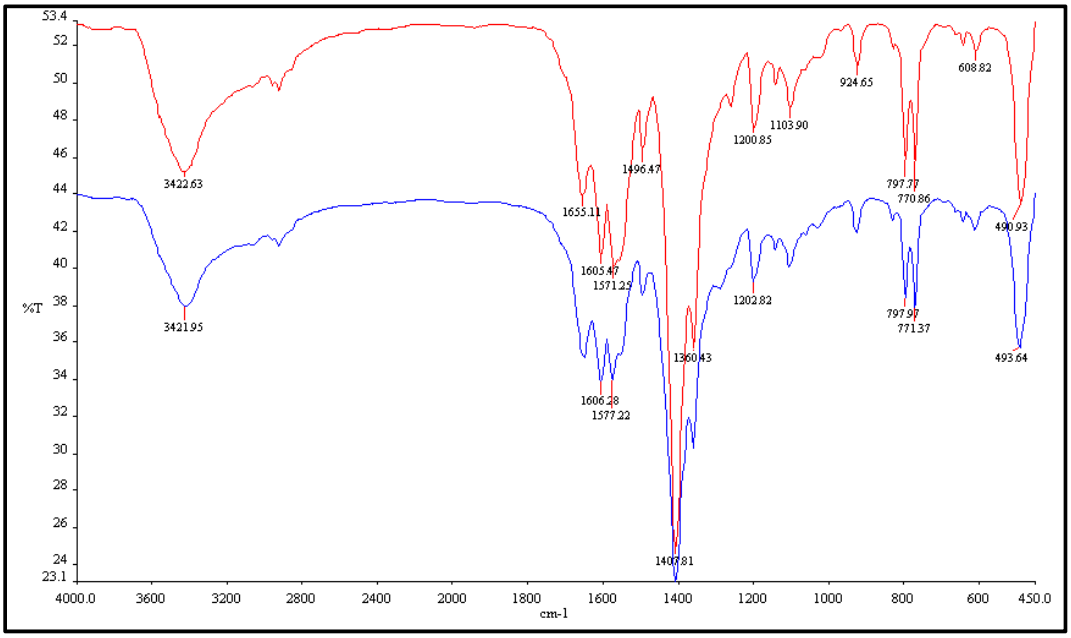


Figure 35: FTIR of Fe-NDC-M (red peaks) and Fe-NDC-O (blue peaks).

## 4.5. Determination of the Loading Efficiencies

The loading efficiencies of calcein disodium salt in Fe-NDC-M and Fe-NDC-O were calculated and are summarized in Tables 1 and 2, respectively. The two MOFs showed successful encapsulation of the model drug with loading efficiencies higher than 98%.

*Note: the fluorescence values were rounded before calculating the loading efficiencies %.

Table 1: Loading efficiencies % of calcein disodium salt in Fe-NDC-M.

| Run | $F_1$ | $F_2$ | Loading efficiency % |
|---|---|---|---|
| **1** | 2.96 | 0.03 | 98.99 |
| **2** | 2.96 | 0.03 | 98.99 |
| **3** | 3.82 | 0.02 | 99.48 |

Table 2: Loading efficiencies % of calcein disodium salt in Fe-NDC-O.

| Run | $F_1$ | $F_2$ | Loading efficiency % |
|---|---|---|---|
| **1** | 3.18 | 0.03 | 99.06 |
| **2** | 3.18 | 0.03 | 99.06 |
| **3** | 3.82 | 0.02 | 99.48 |

### 4.6. Release Experiments

Before starting the release experiments, the power densities were calculated using the equations mentioned in section 3.6. The release percentages of the model drug using the setups explained in the previous chapter (section 3.4) are presented and discussed in the following sections.

**4.6.1. Power densities of the sonication bath and the probe.** The values of the power densities were calculated from the equations listed in section 3.6 and the results are summarized in Table 3.

Table 3: Power densities of the sonication bath and the probe.

| Source and temperature of US | $\bar{V}_{rms}$ (V) | Power density ($W/cm^2$) |
|---|---|---|
| Sonication bath at room temperature | 1.99 | 0.69 |
| Sonication bath at 37°C | 1.86 | 0.61 |
| Probe at room temperature | 1.60 | 0.21 |

**4.6.2. Comparison of calcein release from loaded Fe-NDC-M at 37 ± .0.5 °C without US and after exposure to 40-kHz US.** From Figure 36, it can be seen that the average release percentages increased slightly without US to reach approximately 2.3% after 10 min, whereas it increased significantly after applying 40-kHz US and reached 22.7% after 10 min. This confirms the role of ultrasonic waves in enhancing the oscillation of the nanoparticles which in turns enhances the drug release [41].

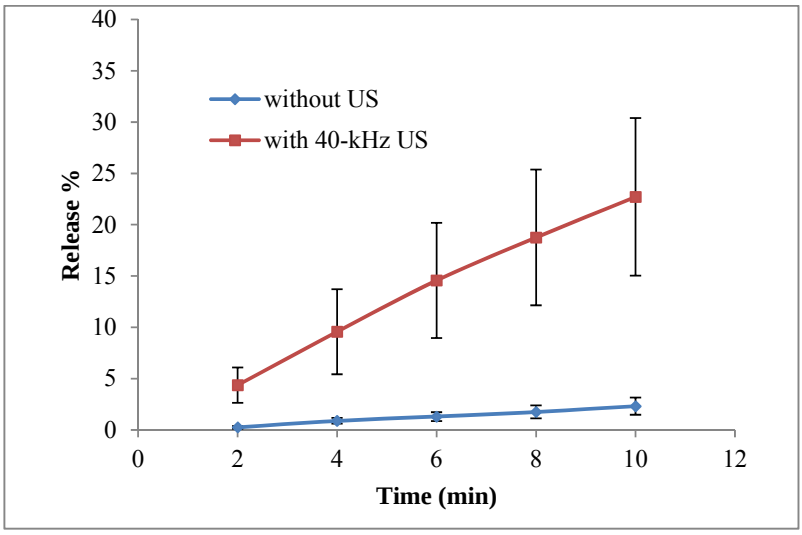


Figure 36: Calcein release from loaded Fe-NDC-M at 37 ± 0.5 °C without US (blue line) and after exposure to 40-kHz US (red line).

Table 4 summarizes the pairwise comparisons. The numbers in the upper right are the Tukey-Kramer minimum significant differences, while the numbers in the lower left are the observed absolute value of the difference in means between each pair of groups. The numbers with asterisks (*) in the lower left indicate the pairs which have significant difference (as they are greater than 9.5192).

*Note: All Tukey-Kramer minimum significant differences were rounded after calculating them from the release percentages which were based on the fluorescence values without rounding.

**4.6.3. Comparison of calcein release from loaded Fe-NDC-M at 37 ± 0.5 °C without US and with exposure to 40-kHz US after vortexing.** As represented in Figure 37, the release percentages of both setups increased with time and reached 18.1 and 21.4 % after vortexing the samples without and with applying US, respectively, after 10 min. The average release percentages were found to be greater without US than after applying 40-kHz US (except at 2 min). However, the difference was very small. Since the mechanisms of interaction between the ultrasound and the nanoparticles is not clear yet [45], it was not been able to explain the actual reason of getting slightly less release in the case of vortexing the samples after they were exposed to US compared to the other setup (without US). As mentioned before that the size of Fe-NDC-M particles is very small, and thus they a have large surface area.

Vortexing the sample might cause back diffusion of calcein after it has been released by the US (due to the large surface area), although this is less likely due the large concentration gradient inside versus outside the carrier.

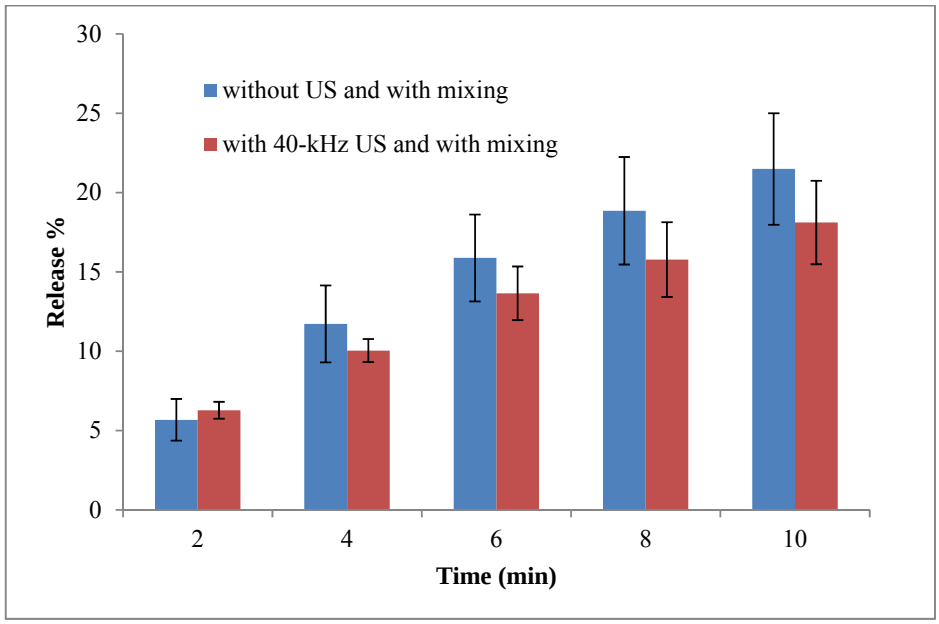


Figure 37: Calcein release from loaded Fe-NDC-M at 37 ± 0.5 °C without US (blue bars) and after exposure to 40-kHz US (red bars) after vortexing.

The results of Tukey-Kramer minimum significant differences are shown in Table 5. The numbers with asterisks (*) in the lower left indicate the significant difference (as they are greater than 5.6578).

**4.6.4. Comparison of calcein release from loaded Fe-NDC-O at 37 ± 0.5 °C without US and after exposure to 40-kHz US.** From Figure 38, we can see a clear upward trend of the release percentages with time for both setups. It was found that without US the release increased slightly and reached approximately 4.9% after 10 min, whereas it increased significantly after applying 40-kHz US to reach 79.7% after 10 min. The US succeeded in triggering the release with a higher percentage after 10 min only.

Table 6 represents the pairwise comparisons of Tukey-Kramer minimum significant differences. The numbers with asterisks (*) in the lower left indicate the significant difference (as they are greater than 5.9183).

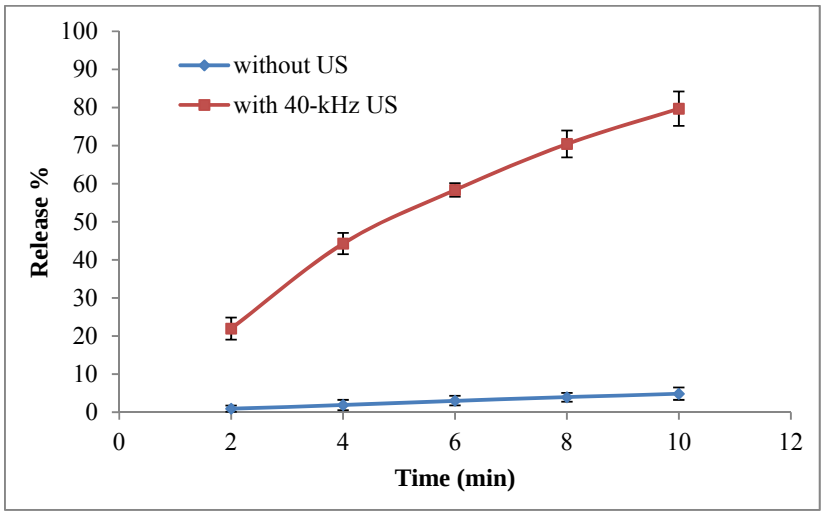


Figure 38: Calcein release from loaded Fe-NDC-O at 37 ± 0.5 °C without US (blue line) and after exposure to 40-kHz US (red line).

**4.6.5. Comparison of calcein release from loaded Fe-NDC-O at 37 ± 0.5 °C without US and with exposure to 40-kHz US after vortexing.** From Figure 39, it can be clearly seen that the release percentages increased with time for both setups. In contrary with the case of Fe-NDC-O, the effect of US in triggering the release was found to be higher (78.9%) than without US (67.7%) after 10 min. This can be attributed to the relatively large sizes (small surface area) of this MOF. In other words, the release was not affected by vortexing the samples and the back diffusion did not occur.

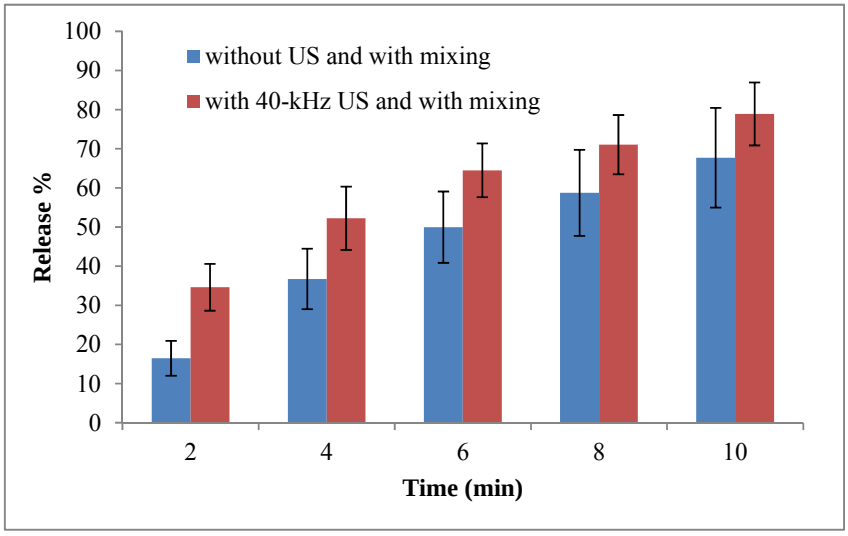


Figure 39: Calcein release from loaded Fe-NDC-O at 37 ± 0.5 °C without US and (blue bars) and with exposure to 40-kHz US (red bars) after vortexing.

Table 4: Tukey-Kramer minimum significant difference for 4 runs of calcein release experiments from loaded Fe-NDC-M at 37 ± 0.5 °C without US and after exposure to 40-kHz US.

| | t=2 no US | t=4 no US | t=6 no US | t=8 no US | t=10 no US | t=2 US | t=4 US | t=6 US | t=8 US | t=10 US |
|---|---|---|---|---|---|---|---|---|---|---|
| t=2 no US | - | 9.5192 | 9.5192 | 9.5192 | 9.5192 | 9.5192 | 9.5192 | 9.5192 | 9.5192 | 9.5192 |
| t=4 no US | 0.6438 | - | 9.5192 | 9.5192 | 9.5192 | 9.5192 | 9.5192 | 9.5192 | 9.5192 | 9.5192 |
| t=6 no US | 1.0449 | 0.401 | - | 9.5192 | 9.5192 | 9.5192 | 9.5192 | 9.5192 | 9.5192 | 9.5192 |
| t=8 no US | 1.5103 | 0.8665 | 0.4655 | - | 9.5192 | 9.5192 | 9.5192 | 9.5192 | 9.5192 | 9.5192 |
| t=10 no US | 2.0669 | 1.4231 | 1.022 | 0.5566 | - | 9.5192 | 9.5192 | 9.5192 | 9.5192 | 9.5192 |
| t=2 US | 4.12 | 3.476 | 3.0752 | 2.6097 | 2.0532 | - | 9.5192 | 9.5192 | 9.5192 | 9.5192 |
| t=4 US | 9.327 | 8.683 | 8.282 | 7.816 | 7.26 | 5.206 | - | 9.5192 | 9.5192 | 9.5192 |
| t=6 US | 14.325* | 13.681* | 13.28* | 12.815* | 12.258* | 10.205* | 4.998 | - | 9.5192 | 9.5192 |
| t=8 US | 18.51* | 17.866* | 17.465* | 16.999* | 16.443* | 14.39* | 9.183 | 4.185 | - | 9.5192 |
| t=10 US | 22.467* | 21.823* | 21.422* | 20.957* | 20.4* | 18.347* | 13.14* | 8.142 | 3.957 | - |

Table 5: Tukey-Kramer minimum significant difference for 4 runs of calcein release experiments from loaded Fe-NDC-M at 37 ± 0.5 °C after vortexing without US and after exposure to 40-kHz US.

| after vortexing | t=2 no US | t=4 no US | t=6 no US | t=8 no US | t=10 no US | t=2 US | t=4 US | t=6 US | t=8 US | t=10 US |
|---|---|---|---|---|---|---|---|---|---|---|
| t=2 no US | - | 5.6578 | 5.6578 | 5.6578 | 5.6578 | 5.6578 | 5.6578 | 5.6578 | 5.6578 | 5.6578 |
| t=4 no US | 6.048* | - | 5.6578 | 5.6578 | 5.6578 | 5.6578 | 5.6578 | 5.6578 | 5.6578 | 5.6578 |
| t=6 no US | 10.204* | 4.156 | - | 5.6578 | 5.6578 | 5.6578 | 5.6578 | 5.6578 | 5.6578 | 5.6578 |
| t=8 no US | 13.174* | 7.125* | 2.9696 | - | 5.6578 | 5.6578 | 5.6578 | 5.6578 | 5.6578 | 5.6578 |
| t=10 no US | 15.807* | 9.759* | 5.603 | 2.6338 | - | 5.6578 | 5.6578 | 5.6578 | 5.6578 | 5.6578 |
| t=2 US | 0.6072 | 5.441 | 9.597* | 12.566* | 15.2* | - | 5.6578 | 5.6578 | 5.6578 | 5.6578 |
| t=4 US | 4.365 | 1.6838 | 5.839* | 8.809* | 11.443* | 3.757 | - | 5.6578 | 5.6578 | 5.6578 |
| t=6 US | 7.978* | 1.9297 | 2.2258 | 5.195 | 7.829* | 7.371* | 3.614 | - | 5.6578 | 5.6578 |
| t=8 US | 10.097* | 4.049 | 0.10651 | 3.0761 | 5.71* | 9.49* | 5.733* | 2.1193 | - | 5.6578 |
| t=10 US | 12.436* | 6.388* | 2.2322 | 0.7374 | 3.371 | 11.829* | 8.072* | 4.458 | 2.3387 | - |

The numbers with asterisks (*) in the lower left of Table 7 indicate Tukey-Kramer minimum significant differences (as they are greater than 20.9262).

**4.6.6. Comparison of calcein release from loaded Fe-NDC-M and Fe-NDC-O at 37 ± 0.5 °C without US.** From Figure 40, it was observed that both MOFs did not show a significant increase in the average release percentages which reached approximately 2.3 and 4.9 % from loaded Fe-NDC-M and Fe-NDC-O, respectively, after 10 min. The release from Fe-NDC-O was relatively high than from Fe-NDC-M. This may indicate a higher porosity of Fe-NDC-O compared to the other MOF (it was not been possible to determine the porosity during the research time as it needs $N_2$ absorption spectrum which was not available at AUS).

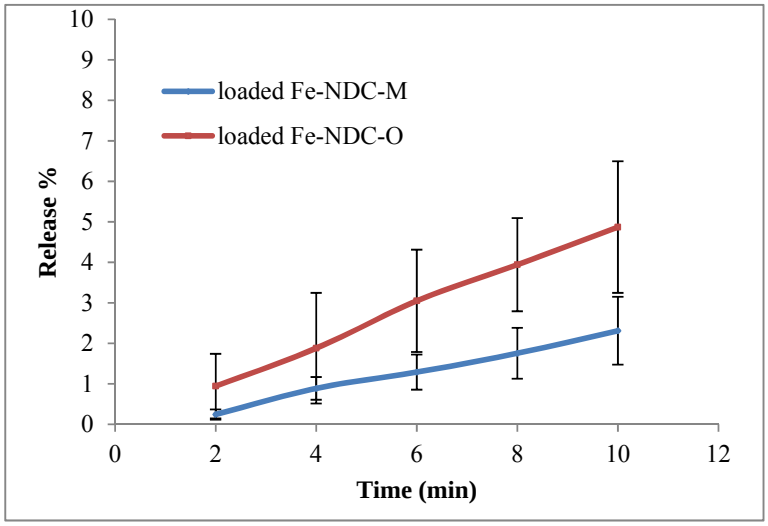


Figure 40: Calcein release from loaded Fe-NDC-M (blue line) and Fe-NDC-O (red line) at 37 ± 0.5 °C without US.

The results of Tukey-Kramer minimum significant differences are shown in Table 8. The numbers with asterisks (*) in the lower left indicate the significant difference (as they are greater than 2.3431).

**4.6.7. Comparison of calcein release from loaded Fe-NDC-M and Fe-NDC-O at 37 ± 0.5 °C after exposure to 40-kHz US.** From the bars shown in Figure 41, it can be clearly seen that the loaded Fe-NDC-O particles released the model drug much faster compared to the loaded Fe-NDC-M during the time intervals. The release percentages from Fe-NDC-M and Fe-NDC-O after 10 min were found to be around

22.7 and 79.7 %, respectively. One possible reason for this increase may be referred to the mechanism of the US (the pore structure tortuosity of Fe-NDC-O might facilitate the penetration of the US more than in the case of the other MOF).

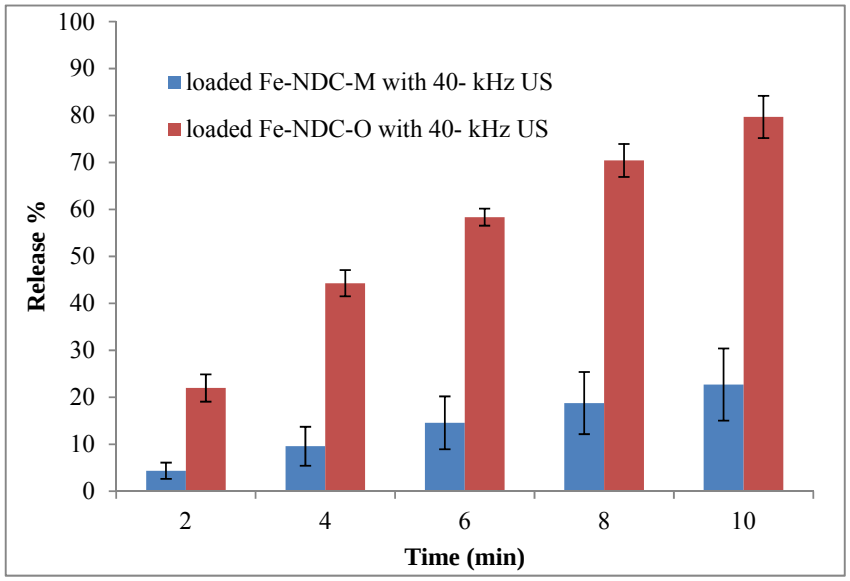


Figure 41: Calcein release from loaded Fe-NDC-M (blue bars) and Fe-NDC-O (red bars) at 37 ± 0.5 °C after exposure to 40-kHz US.

Tukey-Kramer minimum significant differences are summarized in Table 9. The numbers with asterisks (*) in the lower left indicate the significant difference (as they are greater than 10.9613).

**4.6.8. Comparison of calcein release from loaded Fe-NDC-M at room temperature without US and after exposure to 20-kHz US.** From Figure 42, we can see that the effect of the US in triggering the release was significant as it reached 37.5 % after 10 min, while only 1.7% of the drug was released without US. This is another confirmation of the US effect in enhancing the drug release using lower frequency than that used for the previous experiments (40-kHz US).

The results of Tukey-Kramer minimum significant differences are shown in Table 10. The numbers with asterisks (*) in the lower left indicate the significant difference (as they are greater than 14.3071).

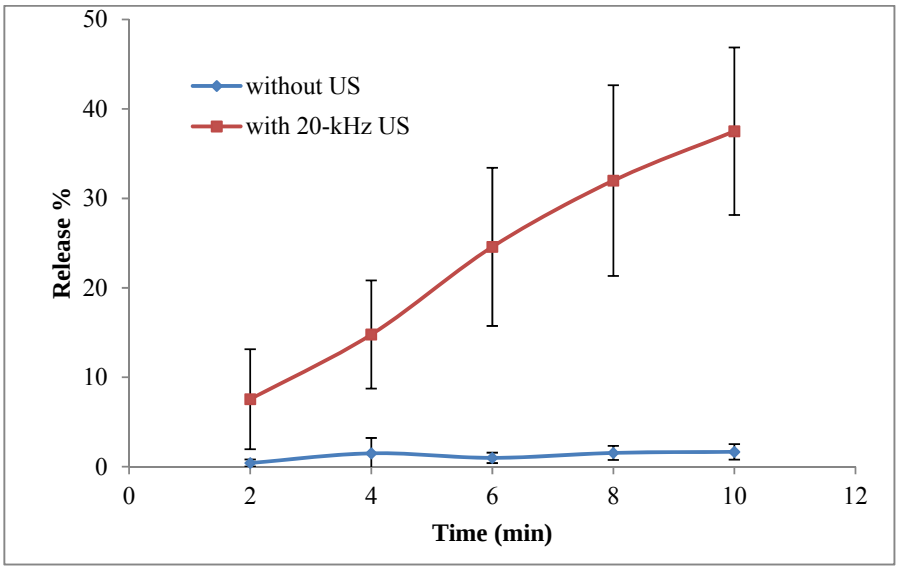


Figure 42: Calcein release from loaded Fe-NDC-M at room temperature without US (blue line) and after exposure to 20-kHz US (red line).

Table 6: Tukey-Kramer minimum significant difference for 4 runs of calcein release experiments from loaded Fe-NDC-O at 37 ± 0.5 °C without US and after exposure to 40-kHz US.

| | t=2 no US | t=4 no US | t=6 no US | t=8 no US | t=10 no US | t=2 US | t=4 US | t=6 US | t=8 US | t=10 US |
|---|---|---|---|---|---|---|---|---|---|---|
| t=2 no US | - | 5.9183 | 5.9183 | 5.9183 | 5.9183 | 5.9183 | 5.9183 | 5.9183 | 5.9183 | 5.9183 |
| t=4 no US | 0.9369 | - | 5.9183 | 5.9183 | 5.9183 | 5.9183 | 5.9183 | 5.9183 | 5.9183 | 5.9183 |
| t=6 no US | 2.1079 | 1.171 | - | 5.9183 | 5.9183 | 5.9183 | 5.9183 | 5.9183 | 5.9183 | 5.9183 |
| t=8 no US | 3.0009 | 2.064 | 0.893 | - | 5.9183 | 5.9183 | 5.9183 | 5.9183 | 5.9183 | 5.9183 |
| t=10 no US | 3.928 | 2.991 | 1.82 | 0.9271 | - | 5.9183 | 5.9183 | 5.9183 | 5.9183 | 5.9183 |
| t=2 US | 21.039* | 20.102* | 18.931* | 18.038* | 17.111* | - | 5.9183 | 5.9183 | 5.9183 | 5.9183 |
| t=4 US | 43.34* | 42.4* | 41.23* | 40.34* | 39.41* | 22.302* | - | 5.9183 | 5.9183 | 5.9183 |
| t=6 US | 57.4* | 56.47* | 55.3* | 54.4* | 53.48* | 36.36* | 14.062* | - | 5.9183 | 5.9183 |
| t=8 US | 69.49* | 68.55* | 67.38* | 66.49* | 65.56* | 48.45* | 26.149* | 12.086* | - | 5.9183 |
| t=10 US | 78.76* | 77.82* | 76.65* | 75.75* | 74.83* | 57.72* | 35.41* | 21.352* | 9.266* | - |

Table 7: Tukey-Kramer minimum significant difference for 4 runs of calcein release experiments from loaded Fe-NDC-O at 37 ± 0.5 °C without US and with exposure to 40-kHz US after vortexing.

| after vortexing | t=2 no US | t=4 no US | t=6 no US | t=8 no US | t=10 no US | t=2 US | t=4 US | t=6 US | t=8 US | t=10 US |
|---|---|---|---|---|---|---|---|---|---|---|
| t=2 no US | - | 20.9262 | 20.9262 | 20.9262 | 20.9262 | 20.9262 | 20.9262 | 20.9262 | 20.9262 | 20.9262 |
| t=4 no US | 20.271 | - | 20.9262 | 20.9262 | 20.9262 | 20.9262 | 20.9262 | 20.9262 | 20.9262 | 20.9262 |
| t=6 no US | 33.5* | 13.23 | - | 20.9262 | 20.9262 | 20.9262 | 20.9262 | 20.9262 | 20.9262 | 20.9262 |
| t=8 no US | 42.27* | 22.001* | 8.772 | - | 20.9262 | 20.9262 | 20.9262 | 20.9262 | 20.9262 | 20.9262 |
| t=10 no US | 51.25* | 30.977* | 17.747 | 8.976 | - | 20.9262 | 20.9262 | 20.9262 | 20.9262 | 20.9262 |
| t=2 US | 22.094* | 1.8227 | 11.407 | 20.179 | 29.155* | - | 20.9262 | 20.9262 | 20.9262 | 20.9262 |
| t=4 US | 40.55* | 20.278 | 7.048 | 1.7233 | 10.699 | 18.455 | - | 20.9262 | 20.9262 | 20.9262 |
| t=6 US | 52.45* | 32.18* | 18.946 | 10.174 | 1.1984 | 30.353* | 11.897 | - | 20.9262 | 20.9262 |
| t=8 US | 57.81* | 37.54* | 24.31* | 15.539 | 6.563 | 35.72* | 17.262 | 5.365 | - | 20.9262 |
| t=10 US | 64.24* | 43.96* | 30.734* | 21.962* | 12.987 | 42.14* | 23.686* | 11.788 | 6.424 | - |

Table 8: Tukey-Kramer minimum significant difference for 4 runs of calcein release experiments from loaded Fe-NDC-M (abbreviated as M) and loaded Fe-NDC-O (abbreviated as O) at 37 ± 0.5 °C without US.

| | t=2,M | t=4,M | t=6,M | t=8,M | t=10,M | t=2,O | t=4,O | t=6,O | t=8,O | t=10,O |
|---|---|---|---|---|---|---|---|---|---|---|
| t=2,M | - | 2.3431 | 2.3431 | 2.3431 | 2.3431 | 2.3431 | 2.3431 | 2.3431 | 2.3431 | 2.3431 |
| t=4,M | 0.6438 | - | 2.3431 | 2.3431 | 2.3431 | 2.3431 | 2.3431 | 2.3431 | 2.3431 | 2.3431 |
| t=6,M | 1.0449 | 0.401 | - | 2.3431 | 2.3431 | 2.3431 | 2.3431 | 2.3431 | 2.3431 | 2.3431 |
| t=8,M | 1.5103 | 0.8665 | 0.4655 | - | 2.3431 | 2.3431 | 2.3431 | 2.3431 | 2.3431 | 2.3431 |
| t=10,M | 2.0669 | 1.4231 | 1.022 | 0.5566 | - | 2.3431 | 2.3431 | 2.3431 | 2.3431 | 2.3431 |
| t=2,O | 0.6984 | 0.05455 | 0.3465 | 0.812 | 1.3685 | - | 2.3431 | 2.3431 | 2.3431 | 2.3431 |
| t=4,O | 1.6353 | 0.9915 | 0.5904 | 0.12495 | 0.4316 | 0.9369 | - | 2.3431 | 2.3431 | 2.3431 |
| t=6,O | 2.8063* | 2.1625 | 1.7615 | 1.296 | 0.7394 | 2.1079 | 1.171 | - | 2.3431 | 2.3431 |
| t=8,O | 3.699* | 3.0555* | 2.6544* | 2.1889 | 1.6324 | 3.0009* | 2.064 | 0.893 | - | 2.3431 |
| t=10,O | 4.626* | 3.983* | 3.581* | 3.116* | 2.5594* | 3.928* | 2.991* | 1.82 | 0.9271 | - |

Table 9: Tukey-Kramer minimum significant difference for 4 runs of calcein release experiments from loaded Fe-NDC-M (abbreviated as M) and loaded Fe-NDC-O (abbreviated as O) at 37 ± 0.5 °C after exposure to 40-kHz US.

| | t=2,M | t=4,M | t=6,M | t=8,M | t=10,M | t=2,O | t=4,O | t=6,O | t=8,O | t=10,O |
|---|---|---|---|---|---|---|---|---|---|---|
| t=2,M | - | 10.9613 | 10.9613 | 10.9613 | 10.9613 | 10.9613 | 10.9613 | 10.9613 | 10.9613 | 10.9613 |
| t=4,M | 5.206 | - | 10.9613 | 10.9613 | 10.9613 | 10.9613 | 10.9613 | 10.9613 | 10.9613 | 10.9613 |
| t=6,M | 10.205 | 4.998 | - | 10.9613 | 10.9613 | 10.9613 | 10.9613 | 10.9613 | 10.9613 | 10.9613 |
| t=8,M | 14.39* | 9.183 | 4.185 | - | 10.9613 | 10.9613 | 10.9613 | 10.9613 | 10.9613 | 10.9613 |
| t=10,M | 18.347* | 13.14* | 8.142 | 3.957 | - | 10.9613 | 10.9613 | 10.9613 | 10.9613 | 10.9613 |
| t=2,O | 17.617* | 12.41* | 7.412 | 3.227 | 0.73 | - | 10.9613 | 10.9613 | 10.9613 | 10.9613 |
| t=4,O | 39.92* | 34.71* | 29.714* | 25.529* | 21.572* | 22.302* | - | 10.9613 | 10.9613 | 10.9613 |
| t=6,O | 53.98* | 48.78* | 43.78* | 39.59* | 35.63* | 36.36* | 14.062* | - | 10.9613 | 10.9613 |
| t=8,O | 66.07* | 60.86* | 55.86* | 51.68* | 47.72* | 48.45* | 26.149* | 12.086* | - | 10.9613 |
| t=10,O | 75.33* | 70.13* | 65.13* | 60.94* | 56.99* | 57.72* | 35.41* | 21.352* | 9.266 | - |

Table 10: Tukey-Kramer minimum significant difference for 4 runs of calcein release experiments from loaded Fe-NDC-M at room temperature without US and after exposure to 20-kHz US.

| | t=2 no US | t=4 no US | t=6 no US | t=8 no US | t=10 no US | t=2 US | t=4 US | t=6 US | t=8 US | t=10 US |
|---|---|---|---|---|---|---|---|---|---|---|
| t=2 no US | - | 14.3071 | 14.3071 | 14.3071 | 14.3071 | 14.3071 | 14.3071 | 14.3071 | 14.3071 | 14.3071 |
| t=4 no US | 1.0865 | - | 14.3071 | 14.3071 | 14.3071 | 14.3071 | 14.3071 | 14.3071 | 14.3071 | 14.3071 |
| t=6 no US | 0.5764 | 0.5101 | - | 14.3071 | 14.3071 | 14.3071 | 14.3071 | 14.3071 | 14.3071 | 14.3071 |
| t=8 no US | 1.1317 | 0.04518 | 0.5552 | - | 14.3071 | 14.3071 | 14.3071 | 14.3071 | 14.3071 | 14.3071 |
| t=10 no US | 1.2519 | 0.16542 | 0.6755 | 0.12024 | - | 14.3071 | 14.3071 | 14.3071 | 14.3071 | 14.3071 |
| t=2 US | 7.132 | 6.046 | 6.556 | 6.001 | 5.88 | - | 14.3071 | 14.3071 | 14.3071 | 14.3071 |
| t=4 US | 14.366* | 13.279 | 13.789 | 13.234 | 13.114 | 7.233 | - | 14.3071 | 14.3071 | 14.3071 |
| t=6 US | 24.166* | 23.08* | 23.59* | 23.035* | 22.915* | 17.034* | 9.801 | - | 14.3071 | 14.3071 |
| t=8 US | 31.574* | 30.488* | 30.998* | 30.443* | 30.322* | 24.442* | 17.209* | 7.408 | - | 14.3071 |
| t=10 US | 37.09* | 36.01* | 36.52* | 35.96* | 35.84* | 29.963* | 22.729* | 12.928 | 5.521 | - |

# Chapter 5. Conclusion and Future Work

Over the past two decades, different nanocarriers have been utilized to target various anti-neoplastic agents. These nanomaterials are non-toxic, stable *in vitro* and *in vivo* environments, biodegradable and have controllable drug distribution and release. One of the recent nanoparticles investigated as effective drug carriers are metal organic frameworks which have well-known crystalline structures and high porosity. They also possess flexibility to be formed and tuned by combining different metal ions with organic ligands to achieve the desired structures and sizes. In this thesis, two new MOFs were prepared from iron nitrate and 2,6 naphthalenedicarboxylic acid using two techniques. The first MOF (Fe-NDC-M) was synthesized in a microwave oven, while the second (Fe-NDC-O) was prepared in a conventional electrical oven. The resulting particles were characterized using X-ray diffraction (XRD), scanning electron microscopy (SEM), energy-dispersive X-ray (EDS) and Fourier transform infrared spectroscopy (FTIR) techniques. The loading efficiencies of calcein disodium salt (a model drug mimicking the anti-neoplastic agent doxorubicin) in both MOFs were calculated to be greater than 98%. Additionally, the drug release behavior was investigated under different conditions. Without ultrasound (US) and at 37°C, the release percentages from the loaded Fe-NDC-M and Fe-NDC-O were found to be 2.3 and 4.9 %, respectively, after 10 min. When the samples were exposed to 40-kHz US, the release percentages increased considerably to reach 22.7 and 79.7 % for Fe-NDC-M and Fe-NDC-O, respectively. Moreover, the loaded Fe-NDC-M was exposed to another US frequency (20-kHz) at room temperature and the release percentage reached 37.5%, whereas it was only 1.7% without US. This is another confirmation of the US effect in enhancing the drug release. The drug delivery system, proposed in this thesis, works by injecting the loaded nanocarriers directly to the tumor site.

Further experiments arising from the findings of this thesis could be pursued. First, changing the solvent, molar ratios of the reactants, temperature and reaction time may produce particles with different structures and sizes. In addition, various concentrations of the model drug can be loaded in the MOFs to investigate the effect of the concentration on the loading efficiency and the release behavior. The release kinetics can be studied in an acidic medium (pH 5.0) to simulate the acidic

environment of the cancer cells. The results can then be compared with those calculated at neutral pH PBS to determine if the MOFs are pH sensitive. Also, the cytotoxicity values of the empty MOFs, free and encapsulated (model drugs and anti-neoplastic agents) can be determined by conducting *in vivo* and *in vitro* experiments. The apoptosis (programmed cell death) and necrosis (rapid and random cell death) can also be studied by treating different cell lines with the loaded MOFs which will help determine the biological mode of cell death. The loaded MOFs can be functionalized by conjugating ligands to their surfaces to produce active-targeting nanocarriers. Finally, all the previous suggestions can be carried out using an actual anti-neoplastic agent (e.g. DOX) instead of the model drug calcein.

# References


[1] A. Sudhakar, "History of Cancer, Ancient and Modern Treatment Methods," *Journal of Cancer Science & Therapy,* vol. 1, no. 2, pp. 1-4, 2009.

[2] A. Jemal, F. Bray, M. M. Center, J. Ferlay, E. Ward and D. Forman, "Global Cancer Statistics," *A Cancer Journal for Clinicians,* vol. 61, no. 2, pp. 69-90, 2011.

[3] D. S. Shewach and R. D. Kuchta, "Introduction to Cancer Chemotherapeutics," *Chemical Reviews,* vol. 109, no. 7, pp. 2859-2861, 2009.

[4] L. A. Torre, F. Bray, R. L. Siegel, J. Ferlay, J. Lortet-Tieulent and A. Jemal, "Global Cancer Statistics, 2012," *A Cancer Journal for Clinicians,* vol. 65, pp. 87-108, 2015.

[5] Ö. U. Sönmez, Z. G. Yalçın, E. Karakeçe, I. H. Çiftci and T. Erdem, "Associations between Demodex species infestation and various types of cancer," *Acta Parasitologica,* vol. 58, no. 4, pp. 551-555, 2013.

[6] R. H. Bradbury , *Cancer*, Alderley Park: Springer-Verlag Berlin Heidelberg, 2007.

[7] B. Pardee, "Cancer Cells and Normal Cells," *American Philosophical Society,* vol. 120, no. 2, pp. 87-92, 1976.

[8] T. Reya, S. J. Morrison, M. F. Clarke and . I. L. Weissman, "Stem cells, cancer, and cancer stem cells," *Nature,* vol. 414, pp. 105-111, 2001.

[9] E. Tran and S. A. Rosenberg, "T-cell therapy against cancer mutations," *Oncotarget,* vol. 5, no. 13, pp. 4579-4580, 2014.

[10] M.G.P.Stoker, "The Leeuwenhoek Lecture, 1971: Tumour Viruses and the Sociology of Fibroblasts," *The Royal Society,* vol. 181, no. 1062, pp. 1-17, 1972.

[11] N. F. Josef and F. Trnka , "Proenzyme Therapy of Cancer," *Anticancer Research,* vol. 25, pp. 1157-1178, 2005.

[12] R. A. Tobey and K. D. Ley, "Iso- leucine Mediated Regulation of Genome Replication in Various Mammalian Cell Lines," *Cancer Research,* vol. 31, pp. 46-51, 1971.

[13] M. R. Chorawala, P. M. Oza and G. B. Shah, "Mechanisms of Anticancer Drugs Resistance: An Overview," *International Journal of Pharmaceutical Sciences and Drug Research ,* vol. 4, no. 1, pp. 1-9, 2012.

[14] Y. H. Bae, R. J. Mrsny and K. Park, Cancer Targeted Drug Delivery: An Elusive Dream, New York: Springer Science+Business Media, 2013.

[15] E. Chu and V. DeVita, "A History of Cancer Chemotherapy," *American Association for Cancer,* vol. 68, no. 21, pp. 8643-8653, 2008.

[16] K. Strebhardt and A. Ullrich, "Paul Ehrlich's magic bullet concept: 100 years of progress," *Nature Reviews Cancer,* vol. 8, pp. 473-480, 2008.

[17] W. Mier, J. Hoffend, U. Haberkorn and M. Eisenhut, "Current Strategies in Tumor-Targeting," in *Apoptotic Pathways as Targets for Novel Therapies in Cancer and Other Diseases*, Heidelberg, Springer, 2005, pp. 343-355.

[18] R. J. Papac, "Origins of Cancer Therapy," *Yale Journal of Biology and Medicine,* vol. 74, pp. 391-398, 2001.

[19] Q. Dong , D. Barsky, M. E. Colvin, C. F. Melius, S. M. Ludeman , J. F. Moravek , O. M. Colvin , D. D. Bigner, P. Modrich and H. S. Friedman, "A structural basis for a phosphoramide mustard-induced DNA interstrand cross-link at 5'-d(GAC)," *Proceedings of the National Academy of Sciences of the United States of America,* vol. 92, no. 26, pp. 12170-12174, 1995.

[20] W. Jacobson, "The Mode of Action of Folic Acid Antagonists on Cells," *J. Physiol. ,* vol. 123, pp. 603-6I7, 1954.

[21] Y. Albushra , A. R. Ahmed and Y. Hasan, "Prevention and Management of High Dose Methotrexate Toxicity," *Journal of Cancer Science & Therapy,* vol. 5, no. 3, pp. 106-112, 2013.

[22] D. B. Longley, D. P. Harkin and P. G. Johnston, "5-Fluorouracil: Mechanisms of Action and Clinical Strategies," *Nature Reviews Cancer,* vol. 3, pp. 330-338, 2003.

[23] G. Tripodo, D. Mandracchia, S. Collina, M. Rui and D. Rossi, "New Perspectives in Cancer Therapy: The Biotin-Antitumor Molecule Conjugates," *Medicinal chemistry,* pp. 1-8, 2014.

[24] X. Wang, S. Li, Y. Shi, X. Chuan, J. Li, T. Zhong, H. Zhang, W. Dai, B. He and Q. Zhang, "The development of site-specific drug delivery nanocarriers based on receptor mediation," *Journal of Controlled Release,* vol. 193, pp. 139-153, 2014.

[25] P. Reschiglian, R. Gref, S. Monti, I. Manet, V. Agostoni, P. Reschigl, R. Gref and S. Monti, "Host−Guest Interactions in Fe(III)-Trimesate MOF Nanoparticles Loaded with Doxorubicin," *Physical Chemistry,* vol. 118, pp. 8532-8539, 2014.

[26] L. Kang, Z. Gao, W. Huang, M. Jin and Q. Wang, "Nanocarrier-mediatedco-delivery of chemotherapeutic drugs and gene agents for cance rtreatment," *Acta Pharmaceutica Sinica B,* vol. 5, no. 3, pp. 169-175, 2015.

[27] J. Agnihotri, S. Saraf and A. Khale, "Targeting : New Potential Carriers for Targeted Drug Delivery System," *International Journal of Pharmaceutical Sciences Review and Research,* vol. 8, no. 2, pp. 117-123, 2011.

[28] M. Kanapathipillai, A. Brock and D. E. Ingber, "Nanoparticle targeting of anti-cancer drugs that alter intracellular signaling or influence the tumor microenvironment," *Advanced Drug Delivery Reviews,* vol. 79–80, pp. 107-118, 2014.

[29] Y. Matsumura and H. Maeda, "A New Concept for Macromolecular Therapeutics in Cancer Chemotherapy: Mechanism of Tumoritropic Accumulation of Proteins and the Antitumor Agent Smancs," *Cancer Research ,* vol. 46, pp. 6387-6392, 1986.

[30] J. Fang, H. Nakamura and H. Maeda, "The EPR effect: Unique features of tumor blood vessels for drug delivery, factors involved, and limitations and augmentation of the effect," *Advanced Drug Delivery Reviews,* vol. 63, pp. 136-151, 2011.

[31] K. R. Jain and T. Stylianopoulos, "Delivering nanomedicine to solid tumors," *Nature Reviews Clinical Oncology,* vol. 7, pp. 653-664, 2010.

[32] A. K. Mishra, *Nanomedicine for Drug Delivery and Therapeutics*, Johannesburg: John Wiley & Sons, 2013.

[33] J. X. Jiang, J. J. Keating, E. M. D. Jesus, R. P. Judy, B. Madajewski, O. Venegas, O. T. Okusanya and S. Singhal, "Optimization of the enhanced permeability and retention effect for near-infrared imaging of solid tumors with indocyanine green," *American Journal of Nuclear Medicine and Molecular Imaging,* vol. 5, no. 4, pp. 390-400, 2015.

[34] N. Bertrand, J. Wu, X. Xu, N. Kamaly and O. C. Farokhzadb, "Cancer nanotechnology: The impact of passive and active targeting in the era of modern cancer biology," *Advanced Drug Delivery Reviews,* vol. 66 , pp. 2-25, 2013.

[35] S. K. Hobbs, W. L. Monsky, F. Yuan, W. G. Roberts, L. Griffith, V. P. Torchilin and R. K. Jain, "Regulation of transport pathways in tumor vessels: Role of tumor type and microenvironment," *Proceedings of the National Academy of Sciences of the United States of America,* vol. 95, no. 8, pp. 4607-4612, 1998.

[36] F. Danhier , O. Feron and V. Préat, "To exploit the tumor microenvironment: Passive and active tumor targeting of nanocarriers for anti-cancer drug delivery," *Journal of Controlled Release,* vol. 148, pp. 135-146, 2010.

[37] S. Keskin and S. Kızılel, "Biomedical Applications of Metal Organic Frameworks," *Industrial and Engineering Chemistry Research,* vol. 50, no. 4, pp. 1799-1812, 2011.

[38] M. R. Ryder and . J. -C. Tan, "Nanoporous metal organic framework materials for smart applications," *Materials Science and Technology,* vol. 30, pp. 1598-1612, 2014.

[39] H. Furukawa, K. E. Cordova, M. O'Keeffe and O. M. Yaghi, "The Chemistry and Applications of Metal-Organic Frameworks," *American Association for the Advancement of Science,* vol. 341, pp. 974-986, 2013.

[40] R. C.Huxford, J. D. Rocca and W. Lin, "Metal-Organic Frameworks as Potential Drug Carriers," *Current Opinion in Chemical Biology,* vol. 14, no. 2, pp. 262-268, 2010.

[41] G. A. Husseini and W. G. Pitt, "Micelles and Nanoparticles for Ultrasonic Drug and Gene Delivery," *Adv Drug Deliv Rev.,* vol. 60, no. 10, pp. 1137-1152, 2008.

[42] S. Ganta, H. Devalapally, A. Shahiwala and M. Amiji, "A review of stimuli-responsive nanocarriers for drug and gene delivery," *Journal of Controlled Release,* vol. 126, pp. 187-204, 2008.

[43] E.-K. Lim , E. Jang , K. Lee, S. Haam and Y.-M. Huh, "Delivery of Cancer Therapeutics Using Nanotechnology," *Pharmaceutics,* vol. 5, pp. 294-317, 2013.

[44] S. Mura, J. Nicolas and P. Couvreur, "Stimuli-responsive nanocarriers for drug delivery," *Nature Materials ,* vol. 12, pp. 991-1003, 2013.

[45] Q.-L. Zhou, Z.-Y. Chen, Y.-X. Wang, F. Yang, Y. Lin and Y.-Y. Liao, "Ultrasound-Mediated Local Drug and Gene Delivery Using Nanocarriers," *BioMed. Research International,* vol. 2014, pp. 1-13, 2014.

[46] B. Hildebrandt , P. Wust, O. Ahlers , G. Sreenivasa, T. Kerner, R. Felix and H. Riess, "The cellular and molecular basis of hyperthermia," *Critical Reviews in Oncology/Hematology,* vol. 43, pp. 33-56, 2002.

[47] H. Grull and S. Langereis, "Hyperthermia-triggered drug delivery from temperature-sensitive liposomes using MRI-guided high intensity focused ultrasound," *Journal of Controlled Release,* vol. 161, pp. 317-327, 2012.

[48] M. Thanou and W. Gedroyc, "MRI-Guided Focused Ultrasound as a New Method of Drug Delivery," *Journal of Drug Delivery,* vol. 2013, pp. 1-12, 2013.

[49] K. G. Baker, V. J. Robertson and F. A. Duck, "A Review of Therapeutic Ultrasound: Biophysical Effects," *Physical Therapy,* vol. 81, pp. 1351-1358, 2001.

[50] L. R. Macgillivray, *Metal-Organic Frameworks: Design and Application*, New Jersy: John Wiely & Sons,Inc., 2010.

[51] H.-C. Zhou, J. R. Long and O. M. Yaghi, "Introduction to Metal−Organic Frameworks," *Chemical Reviews,* vol. 112, no. 2, pp. 673-674, 2012.

[52] C. Dey, T. Kundu, B. P. Biswal, A. Mallick and R. Banerjee, "Crystalline metal-organic frameworks (MOFs): synthesis, structure and function," *Acta Crystallographica Section B,* vol. 70, pp. 3-10, 2013.

[53] S. Mukherjee and M. A. Vannice, "Solvent effects in liquid-phase reactions: I. Activity and selectivity during citral hydrogenation on Pt/SiO2 and evaluation of mass transfer effects," *Journal of Catalysis,* vol. 243, no. 1, pp. 108-130, 2006.

[54] R. Gani, . C. Jiménez-González and D. J. Constable, "Method for selection of solvents for promotion of organic reactions," *Computers and Chemical Engineering,* vol. 29, no. 7, pp. 1661-1676, 2005.

[55] B. F. Hoskins and R. Robson, "Infinite polymeric frameworks consisting of three dimensionally linked rod-like segments," *Journal of The American Chemical Society,* vol. 111, pp. 5962-5964, 1989.

[56] M. Fujita, Y. J. Kwon, S. Washizu and O. Katsuyuki, "Preparation, Clathration Ability, and Catalysis of a Two-Dimensional Square Network Material Composed of Cadmium( 11) and 4,4' Bipyridine," *Journal of American Chemical Society,* vol. 116, no. 3, pp. 1151-1152, 1994.

[57] M. Wysokowski, K. Materna, J. Walter , I. Petrenko, A. L. Stelling, V. V. Bazhenov, L. Klapiszewski, T. Szatkowski, O. Lewandowska, D. Stawski, S. L. Molodtsov, H. Maciejewski, H. Ehrlich and T. Jesionowski, "Solvothermal synthesis of hydrophobic chitin–polyhedral oligomeric silsesquioxane (POSS) nanocomposites," *International Journal of Biological Macromolecules,* vol. 78, pp. 224-229, 2015.

[58] R. J. Kupplera, D. J. Timmonsb, Q. R. Fan, J.-R. Li, T. A. Makal, M. D. Younga, D. Yuan, D. Zhaoa, W. Zhuang and . H.-C. Zhou, "Potential applications of metal-organic frameworks," *Coordination Chemistry Reviews,* vol. 253, pp. 3042-3066, 2009.

[59] S. Subramanian and M. J. Zaworotko, "Porous Solids by Design: [Zn(4,4′-bpy)2(SiF6)]n·xDMF, a Single Framework Octahedral Coordination Polymer with Large Square Channels," *Angewandte Chemie International Edition,* vol. 34, no. 19, pp. 2127-2129, 1995.

[60] 0. M. Yaghi and H. Li, "Hydrothermal Synthesis of a Metal-Organic Framework Containing Large Rectangular Channels," *Journal of the American Chemical Society,* vol. 117, pp. 10401-10402, 1995.

[61] Z. Ni and R. I. Masel, "Rapid Production of Metal-Organic Frameworks via Microwave-Assisted Solvothermal Synthesis," *Journal of the American Chemical Society,* vol. 128, no. 38, pp. 12394-1239, 2006.

[62] N. Stock and S. Biswas, "Synthesis of Metal-Organic Frameworks (MOFs): Routes to Various MOF Topologies, Morphologies, and Composites," *Chemical Reviews,* vol. 112, no. 2, pp. 933-969, 2012.

[63] R. Ameloot and L. Stappers, "Patterned growth of metal-organic framework coatings by electrochemical synthesis," *Chemistry of Materials,* vol. 21, no. 13, pp. 2580-2582, 2009.

[64] M. Klimakow, P. Klobes and A. F. Thünemann, "Mechanochemical Synthesis of Metal-Organic Frameworks: A Fast and Facile Approach toward Quantitative Yields and High Specific Surface Areas," *Chemistry of Materials,* vol. 22, no. 18, pp. 5216-5221, 2010.

[65] K. S. Suslick and G. J. Price, "Applications of Ultrasound to materials chemistry," *Annual Review of Materials Science,* vol. 29, pp. 295-326, 1999.

[66] P. Horcajada, C. Serre, M. Vallet-Regi, M. Sebban, F. Taulelle and G. Féry, "Metal–Organic Frameworks as Efficient Materials for Drug Delivery," *Angewandte Chemie International Edition,* vol. 45, pp. 5974-5978, 2006.

[67] R. C. Huxford, J. D. Rocca and W. Lin, "Metal-Organic Frameworks as Potential Drug Carriers," *Current Opinion in Chemical Biology,* vol. 14, no. 2, pp. 262-268, 2010.

[68] J. An, S. J. Geib and N. L. Rosi, "Cation-triggered drug release from a porous zinc-adeninate metal–organic framework," *The American Chemical Society,* vol. 131, pp. 8376-8377, 2009.

[69] M. Schäfer-Korting, *Drug Delivery*, Berlin: Springer-Verlag Berlin Heidelberg, 2010.

[70] P. Horcajada, T. Chalati, C. Serre, B. Gillet, C. Sebr, T. Baati, J. F. Eubank, D. Heurtaux, C. Clayette, C. Kreuz, J.-S. Chang, Y. K. Hwang, V. Marsaud, P.-N. Bories, L. Cynober, S. Gil, G. Férey, P. Couvreur and R. Gref, "Porous metal–organic-framework nanoscalecarriers as a potential platform for drug delivery and imaging," *Nature Materials,* vol. 9, pp. 172-178, 2010.

[71] K. M. L. Taylor-Pashow, J. D. Rocca, Z. Xie, S. Tran and W. Lin, "Post-Synthetic Modifications of Iron-Carboxylate Nanoscale Metal-Organic Frameworks for Imaging and Drug Delivery," *American Chemical Society,* vol. 131, pp. 14261-14263, 2009.

[72] N. Graf and S. J. Lippard, "Redox activation of metal-based prodrugs as a strategy for drug delivery," *Advanced Drug Delivery Reviews,* vol. 64, no. 11, pp. 993-1004, 2012.

[73] A.-. M. Florea and D. Büsselberg, "Cisplatin as an Anti-Tumor Drug: Cellular Mechanisms of Activity, Drug Resistance and Induced Side Effects," *Cancers,* vol. 3, pp. 1351-1371, 2011.

[74] G.-. S. Wang, H.-. Y. Zhang and Y. Liu, "Preparation and characterization of inclusion complexes of topotecan with sulfonatocalixarene," *Journal of Inclusion Phenomena And Macrocyclic Chemistry,* vol. 69, pp. 85-89, 2011.

[75] M. Nunzio, V. Agostoni, B. Cohen], R. Gref and A. Douhal, "A “Ship in a Bottle” Strategy To Load a Hydrophilic Anticancer Drug in Porous Metal Organic Framework Nanoparticles: Efficient Encapsulation, Matrix Stabilization, and Photodelivery," *Journal of Medicinal Chemistry,* vol. 57, no. 2, pp. 411-420, 2014.

[76] X. Huang and C. S. Brazel, "On the importance and mechanisms of burst release in matrix-controlled drug delivery systems," *Journal of Controlled Release,* vol. 73, no. 2-3, pp. 121-136, 2001.

[77] B. S. Andersson, M. d. Lima, P. F. Thall, X. Wang, D. Couriel, M. Korbling, S. Roberson, S. G. Giralt, B. Pierre, J. A. Russell, E. J. Shpall, R. B. Jo and R. E. Champlin, "Once Daily i.v. Busulfan and Fludarabine (i.v. Bu-Flu) Compares Favorably with i.v. Busulfan and Cyclophosphamide (i.v. BuCy2) as Pretransplant Conditioning Therapy in AML/MDS," *Biology of Blood and Marrow Transplantation,* vol. 14, pp. 672-684, 2008.

[78] Q. Mei, F. Li, H. Quan, Y. Liu and H. Xu, "Busulfan inhibits growth of human osteosarcoma through miR-200 family microRNAs in vitro and in vivo," *Cancer Science,* vol. 105, no. 7, pp. 755-762, 2014.

[79] T. Chalat, P. Horcajada, P. Couvreur, C. Serre and M. B. Yahia, "Porous metal organic framework nanoparticles to address the challenges related to busulfan encapsulation," *Nanomedicine,* vol. 6, no. 10, pp. 1683-1695, 2011.

[80] G. Takemura and H. Fujiwara, "Doxorubicin-Induced Cardiomyopathy From the Cardiotoxic Mechanisms to Management," *Progress in Cardiovascular Diseases,* vol. 49, no. 5, pp. 330-352, 2007.

[81] Z. Liu, R. Cheung, X. Y. Wu, J. R. Ballinger, R. Bendayan and A. M. Rauth, "A study of doxorubicin loading onto and release from sulfopropyl dextran ion-exchange microspheres," *Journal of Controlled Release,* vol. 77, no. 3, pp. 213-224, 2001.

[82] K. Chatterjee, J. Zhang, N. Honbo and J. S. Karliner, "Doxorubicin Cardiomyopathy," *Cardiology,* vol. 115, no. 2, pp. 155-162, 2010.

[83] Y. Chen, Y. Wan, Y. Wang, H. Zhang and Z. Jiao, "Anticancer efficacy enhancement and attenuation of side effects of doxorubicin with titanium dioxide nanoparticles," *International Journal of Nanomedicine,* vol. 6, pp. 2321-2326, 2011.

[84] R. Krishna and L. D. Mayer, "Multidrug Resistance (MDR) in Cancer - Mechanisms, Reversal Using Modulators of MDR and the Role of MDR Modulators in Influencing the Pharmacokinetics of Anticancer Drugs," *European Journal of Pharmaceutical Sciences,* vol. 11, no. 4, pp. 265-283, 2000.

[85] J. Zhuang, . C.-H. Kuo, L.-Y. Chou, D.-Y. Liu, E. Weerapana and C.-K. Tsung, "Optimized metal organic-framework nanospheres for drug delivery: evaluation of small-molecule encapsulation," *ACS Nano,* vol. 8, no. 3, pp. 2812-2819, 2014.

[86] C.-Y. Sun, C. Qin, X.-L. Wang, G.-S. Yang, K.-Z. Shao, Y.-Q. Lan, Z.-M. Su, P. Huang, C.-G. Wang and E.-B. Wang, "Zeolitic imidazolate framework-8 as efficient pH-sensitive drug delivery vehicle," *Dalton Transactions,* vol. 41, no. 23, pp. 6906-6909, 2012.

[87] J. L. Arias, "Novel strategies to improve the anticancer action of 5-fluorouracil by using drug delivery systems," *Molecules,* vol. 13, pp. 2340-2369, 2008.

[88] K. S. Park, Z. Ni, A. P. Cote, J. Y. Choi, R. Huang, F. J. Uribe-Romo, H. K. Chae, M. and O. M. , "Exceptional chemical and thermal stability of zeolitic imidazolate frameworks," *Proceedings of the National Academy of Sciences of the United States of America,* vol. 103, no. 27, pp. 10186-10191, 2006.

[89] C. Adhikar, A. Das and A. Chakrabort, "Zeolitic imidazole framework (ZIF) nanospheres for easy encapsulation and controlled release of an anticancer drug doxorubicin under different external stimuli: a way toward smart drug delivery system," *Molecular Pharmaceutics,* vol. 12, no. 9, pp. 3158-3166, 2015.

[90] J. Shen, Q. He, Y. Gao, J. Shi and Y. Li, "Mesoporous silica nanoparticles loading doxorubicin reverse multidrug resistance: performance and mechanism," *Nanoscale,* vol. 3, pp. 4314-4322, 2011.

[91] M. Zheng, S. Liu, X. Guan and Z. Xie, "One-Step Synthesis of Nanoscale Zeolitic Imidazolate Frameworks with High Curcumin Loading for Treatment

of Cervical Cancer," *ACS Applied Materials and Interfaces,* vol. 7, no. 40, pp. 22181-22187, 2015.

[92] M. K. Shanmugam , G. Rane, . M. M. Kanchi , F. Arfuso, A. Chinnathambi , M. E. Zayed , B. K. Tan, A. P. Kumar and G. Sethi, "The Multifaceted Role of Curcumin in Cancer Prevention and Treatment," *Molecules ,* vol. 20, pp. 2728-2769, 2015.

[93] P. Anand, A. B. Kunnumakkara, R. A. Newman and B. B. Aggarwal, "Bioavailability of Curcumin: Problems and Promises," *Molecular Pharmaceutics,* vol. 4, no. 6, pp. 807-818, 2007.

[94] S. F. Chin, K. S. Iyer, M. Saunders, T. G. Pierre, C. Buckley, M. Paskevicius and C. L. Raston, "Encapsulation and Sustained Release of Curcumin using Superparamagnetic Silica Reservoirs," *Chemistry - A European Journal,* vol. 15, pp. 5661-5665, 2009.

[95] S. Mourtas , A. N. Lazar , E. Markoutsa and C. Duyckaerts, "Multifunctional nanoliposomes with curcumine-lipid derivative and brain targeting functionality with potential applications for Alzheimer disease," *European Journal of Medicinal Chemistry,* vol. 80 , pp. 175-183, 2014.

[96] A. Sahu, N. Kasoju and U. Bora, "Fluorescence Study of the Curcumin-Casein Micelle Complexation and Its Application as a Drug Nanocarrier to Cancer Cells," *Biomacromolecules,* vol. 9, pp. 2905-2912, 2008.

[97] H. Zheng, Y. Zhang, L. Liu, W. Wan, P. Guo, A. M. Nystrom and X. Zou, "One-pot Synthesis of Metal−Organic Frameworks with Encapsulated Target Molecules and Their Applications for Controlled Drug Delivery," *Journal of the American Chemical Society,* vol. 138, pp. 962-968, 2016.

[98] T. Kundu, S. Mitra, P. Patra, A. Goswami, D. D. Diaz and R. Banerjee, "Mechanical Downsizing of a Gadolinium(III)-based Metal-Organic Framework for Anticancer Drug Delivery," *Chemistry - A European Journal,* vol. 20, pp. 10514-10518, 2014.

[99] G. Long , M. E. Meek and M. Lewis, "N,N-Dimethylformamide," World Health Organization, Geneva, 2001.

[100] F. Ke, Y.-P. Yuan, L.-G. Qiu, Y.-H. Shen, A.-J. Xie, J.-F. Zhu, X.-Y. Tian and L.-D. Zhang, "Facile fabrication of magnetic metal–organic framework nanocomposites for potential targeted drug delivery," *Journal of Materials Chemistry,* vol. 21, no. 11, pp. 3843-3848, 2011.

[101] L. A. Tran and L. J. Wilson, "Nanomedicine: making controllable magnetic drug delivery possible for the treatment of breast cancer," *Breast Cancer Research,* vol. 13, no. 2, p. 303, 2011.

[102] K. D. Rainsford, *Nimesulide – Actions and Uses*, Sheffield: Birkhäuser Basel, 2005.

[103] Z. Liang, J. Liu, L. Li, H. Wang, C. Zhao, L. Jiang and G. Qin, "Effect of nimesulide on the growth of human laryngeal squamous cell carcinoma," *American Journal of Otolaryngology,* vol. 35, no. 2, pp. 120-129, 2014.

[104] M. Mikhaylova, D. K. Kim, N. Bobrysheva, M. Osmolowsky, V. Semenov, T. Tsakalakos and M. Muhammed, "Superparamagnetism of Magnetite Nanoparticles: Dependence on Surface Modification," *Langmuir ,* vol. 20, pp. 2472-2477, 2004.

[105] T. Gadzikwa, G. Lu, C. L. Stern, S. R. Wilson, J. T. Hupp and S. T. Nguyen, "Covalent surface modification of a metal–organic framework: selective surface engineering via CuI-catalyzed Huisgen cycloaddition," *Chemical Communications,* no. 43, pp. 5493-5495, 2008.

[106] S. Das, D. K. Sharma, S. Chakrabarty, A. Chowdhury and S. S. Gupta, "Bioactive Polymersomes Self-Assembled from Amphiphilic PPO-GlycoPolypeptides: Synthesis, Characterization, and Dual-Dye," *Langmuir,* vol. 31, pp. 3402-3412, 2015.

[107] C. A. Orellana-Tavra, E. F. Baxter, T. Tian, T. D. Bennett, N. K. H. Slater, A. K. Cheethamb and D. Fairen-Jimenez, "Amorphous metal-organic frameworks for drug delivery," *Chemical Communication,* vol. 51, no. 73, pp. 13878-13881, 2015.

[108] M. Buczkowski, A. G. Marquez, A. Demessence, A. E. Platero-Prats, D. Heurtaux, P. Horcajada, C. Serre, J.-S. Chang, G. Ferey, A. V. de la Peña-O'Shea, C. Boissiere, D. Grosso, . C. Sanchez and C. Sanchez, "Green Microwave Synthesis of MIL-100(Al, Cr, Fe) Nanoparticles for Thin-Film Elaboration," *European Journal of Inorganic Chemistry,* vol. 2012, no. 32, pp. 5165-5174, 2012.

[109] M. Alhamami, H. Doan and C.-H. Cheng, "A Review on Breathing Behaviors of Metal-Organic-Frameworks (MOFs) for Gas Adsorption," *Materials,* vol. 7, pp. 3198-3250, 204.

[110] E. D. Dikio and A. M. Farah, "Synthesis, Characterization and Comparative Study of Copper and Zinc Metal Organic Frameworks," *Chemical Science Transactions,* vol. 2, no. 4, pp. 1386-1394, 2013.

[111] D. E. Newbury and N. W. M. Ritchie, "Performing elemental microanalysis with high accuracy and high precision by scanning electron microscopy/silicon drift detector energy-dispersive X-ray spectrometry (SEM/SDD-EDS)," *Journal of Materials Science,* vol. 50, pp. 493-518, 2015.

[112] X. Zhang, P. F. Luckham, A. D. Hughes, S. Thom and X. Y. Xu, "Towards an understanding of the release behavior of temperature-sensitive liposomes: a possible explanation of the ‘‘pseudoequilibrium’’ release behavior at the phase transition temperature," *Journal of Liposome Research,* vol. 23, no. 3, pp. 167-173, 2013.

[113] S. Hamann, J. F. Kiilgaard, T. Litman, F. J. Alvarez-Leefmans, B. R. Winther and T. Zeuthen, "Measurement of Cell Volume Changes by Fluorescence Self-Quenching," *Journal of Fluorescence,* vol. 12, no. 2, pp. 139-145, 2002.

[114] G. A. Husseini, M. A. Diaz de la Rosa, T. Gabuji, Y. Zeng, D. A. Christensen and W. G. Pitt, "Release of Doxorubicin from Unstabilized and Stabilized Micelles Under the Action of Ultrasound," *Journal of Nanoscience and Nanotechnology,* vol. 7, no. 3, pp. 1028-1033, 2007.

[115] S. E. Gratton, P. A. Ropp, P. D. Pohlhaus, J. C. Luft, V. J. Madden, M. E. Napier and J. M. DeSimone, "The effect of particle design on cellular internalization pathways," *Proceedings of the National Academy of Sciences of the United States of America,* vol. 105, no. 33, pp. 11613-11618, 2008.

[116] S. Baruaa, J.-W. Yoob, P. Kolhara, A. Wakankar, Y. R. Gokarnc and S. Mitragotri, "Particle shape enhances specificity of antibody-displaying nanoparticles," *Proceedings of the National Academy of Sciences of the United States of America,* vol. 110, no. 9, pp. 3270-3275, 2013.

[117] E. D. Dikio and A. M. Farah, "Synthesis, Characterization and Comparative Study of Copper and Zinc Metal Organic Frameworks," *Chemical Science Transactions,* vol. 2, no. 4, pp. 1386-1394, 2013.

# Vita

Mihad Ibrahim was born in 1989, in Doha, Qatar. After a year, she moved with her family to Sudan where she grew up and earned most of her education. She graduated from Al Manar Al Gadeed High School. In 2011, she received the degree of Bachelor in Chemical Engineering from the University of Khartoum with the first class honor. After that, she worked at the same university as a tutor for 2 years.

In 2013, Ms. Ibrahim was granted an assistantship from the American University of Sharjah in United Arab Emirates. She worked there for 2 years as a graduate teaching assistant while doing her Master's in Chemical Engineering. Then, she continued as a graduate research assistant for one semester.